Microstructural Control in Fabricating Multifunctional Carbon Fibers

by

Rahul Joseph Franklin

A Dissertation Presented in Partial Fulfillment
of the Requirements for the Degree
Master of Science

Approved March 2020 by
Graduate Supervisory Committee:

Kenan Song, Co-Chair
Yang Jiao, Co-Chair
Yongming Liu

ARIZONA STATE UNIVERSITY

May 2020

ABSTRACT

Precursors of carbon fibers include rayon, pitch, and polyacrylonitrile fibers that can be heat-treated for high-strength or high-modulus carbon fibers. Among them, polyacrylonitrile has been used most frequently due to its low viscosity for easy processing and excellent performance for high-end applications. To further explore polyacrylonitrile-based fibers for better precursors, in this study, carbon nanofillers were introduced in the polymer matrix to examine their reinforcement effects and influences on carbon fiber performance. Two-dimensional graphene nanoplatelets were mainly used for the polymer reinforcement and one-dimensional carbon nanotubes were also incorporated in polyacrylonitrile as a comparison. Dry-jet wet spinning was used to fabricate the composite fibers. Hot-stage drawing and heat-treatment were used to evolve the physical microstructures and molecular morphologies of precursor and carbon fibers. As compared to traditionally used random dispersions, selective placement of nanofillers was effective in improving composite fiber properties and enhancing mechanical and functional behaviors of carbon fibers. The particular position of reinforcement fillers with polymer layers was enabled by the in-house developed spinneret used for fiber spinning. The preferential alignment of graphitic planes contributed to the enhanced mechanical and functional behaviors than those of dispersed nanoparticles in polyacrylonitrile composites. The high in-plane modulus of graphene and the induction to polyacrylonitrile molecular carbonization/graphitization were the motivation for selectively placing graphene nanoplatelets between polyacrylonitrile layers. Mechanical tests, scanning electron microscopy, thermal, and electrical properties were characterized. Applications such as volatile organic compound sensing and pressure sensing were demonstrated.

Dedicated to my family.

ACKNOWLEDGMENTS

First, I would like to thank my advisor, Dr. Kenan Song, for letting me join his group to gain valuable experience in a state-of-the-art research lab, for all the help and advice he has lent me these past two years and for supporting me throughout this thesis project. I am grateful for his patience and guidance.

I would also like to thank my co-chair, Dr. Yang Jiao, and committee member, Dr. Yongming Liu, for helping me complete my dissertation. I would like to convey my heartfelt gratitude to my labmates, Weiheng Xu, Dharneedar Ravichandran, Sayli Jambulkar, Namrata Kanth, Amm Hasib, and Yuxiang Zhu for their constant support and encouragement throughout this project. I would especially like to thank Weiheng Xu for his immense contribution to my work. His knowledge of fiber synthesis and its characterization, the training to use several instruments, the inputs to my experimental processes, and, the overall support towards my work has enabled me to complete this thesis in a timely fashion. I would like to thank Dharneedar Ravichandran for his help with the SEM, Raman spectrometer, and for being a friend.

I would like to acknowledge the staff at ASU, who have helped me with the supplies and equipment access that contributed towards my research. This project would not have gone smoothly without their diligent services.

Finally, I would like to thank my family, who have been my bedrock since the very beginning, without whose love, support, and encouragement, I wouldn't have made it this far.

TABLE OF CONTENTS

Page

CHAPTER Page

LIST OF TABLES

Table Page

LIST OF FIGURES

FIGURE PAGE

FIGURE PAGE

LIST OF SYMBOLS

$P(\sigma)$	Probability of failure
R^2	Linear coefficient
x_o	Scale parameter
β	Weibull modulus/ shape parameter
σ	Failure strength
W_0	Initial weight
W_f	Final weight
t	Time

LIST OF ABBREVIATIONS

BNNT	Boron nitride nanotubes
CFs	Carbon fibers
CNCs	Cellulose nanocrystal
CNTs	Carbon nanotubes
DMF	Dimethylformamide
GNP	Graphene nanoplatelets
GNR	Graphene nanoribbon
Grp	Graphene
LCGO	Liquid crystalline graphene oxide
PAN	Polyacrylonitrile
PA6	Polyamide
pCFs	Pre-carbon fibers
PEO	Polyethylene oxide
PMMA	Polymethyl-methacrylate
PS	Polystyrene
PVA	Polyvinyl alcohol
SEM	Scanning electron microscope
VOCs	Volatile organic compounds

Chapter 1. Introduction

1. Carbon fibers

Carbon fibers (CFs) are defined as fibers with diameters of 5–50 μm and carbon content > 90 wt%[1,2]. CFs are an increasingly growing field of interest for their use in aerospace, automobile, defense weapons, civil engineering, sports goods, energy systems and other high-end applications[3] due to their high specific strength and modulus, low density, low thermal expansion or shrinkage, high chemical resistance, and temperature tolerances[4] (**Figure 1**). Macromolecular materials going through a pyrolyzing reaction that leaves high-percentage carbon residue upon heat-treatment in a series of oxide and inert atmospheres are preferred precursors to CFs (pCFs)[5]. After the heat-treatment, the carbon atoms are bonded together in crystals, forming graphitic sheets interlocked with one another, which are more or less aligned parallel to the long axis of the CFs. The crystal alignment gives the fiber high-stiffness, and the elimination of defects during fiber synthesis renter high-strength. The crystal alignment and the defects density depend on the choices of precursors. For example, polyacrylonitrile (PAN)-derived CFs are more turbostratic, with sheets of carbon atoms haphazardly folded or crumpled together. In contrast, mesophase pitch-based CFs contain more graphitic layers after heat treatment at temperatures exceeding 2200 °C. Other precursors may possess hybrid structures with both graphitic and turbostratic parts present. Turbostratic structures tend to produce high tensile strength due to the layer interactions, whereas heat-treated mesophase-pitch-derived carbon fibers have high Young's modulus and high thermal conductivity due to graphitic smoothness. As compared to other precursor polymers (e.g., rayon, lignin, pitch), PAN

depending on chemical synthesis gives higher flexibility of molecular weight manipulations, better control of rheology behaviors during spinning, precise control of fiber sizes and surface coatings, excellent mechanical properties, and higher carbon yield thus has the most attention in carbon fiber synthesis.

Rayon is a cellulose-based material instead of synthetic polymers (**Figure 2a**). Purified cellulose can be harvested from wood pulp and chemically converted into a soluble compound for rayon fibers. Rayon threads were the first pCFs to be pyrolyzed to form CFs back to the 1960s. However, that process proved to be inefficient, as the resulting fibers contained only about 20% carbon and had low strength and stiffness properties. CF manufactured from this precursor material tends to have superior thermal stability but lower mechanical properties[6]. Today less than 2% of CFs are manufactured using this precursor[7]. Unlike other pCFs, rayon-based fibers need not be oxidized to render it infusible; however, oxidation was still done to increase carbon yield.

Lignin is one of the most abundantly available biomolecules on earth that can be extracted from wood, bark, or plant in the cell walls. For example, lignin constitutes 20 to 35% of the dry mass of wood and is easily found as byproducts from paper industries[8]. Chemically, lignins are cross-linked phenolic polymers, with abundant aromatic subunits and hydrophobic features (**Figure 2b**). The degree of polymerization is difficult to measure since the material is heterogeneous. Different types of lignin have been described depending on the means of isolation. Pyrolysis of lignin during the combustion of wood or

charcoal production yields a range of products, of which the most characteristic ones are methoxy-substituted phenols[9]. However, researchers recently have been trying to convert lignin to convert into carbon fibers. Lignin is blended with polymeric materials, such as polyethylene oxide (PEO), for synthesizing lignin-based fibers. These fibers can be pyrolyzed to remove volatile content, which is the source of a majority of defects in lignin-based carbon fibers, and to covert the thermal properties from thermoplastic materials to thermosetting carbon fibers[10,11].

Pitch is obtained in the form of (i) the petroleum pitch, a byproduct of the petroleum distillation process, (ii) the coal tar pitch, or (iii) plants, all of which are highly aromatic compounds[12]. Various forms of pitch may also be called tar, bitumen, or asphalt, among which tar is more seen as liquid and pitch more as solid-state. Among different sources to obtain pitch, the petroleum pitch is much more attractive as a precursor material for carbon fibers. Pitch is thermoplastic and can be melt-spun into fibers. When pitches are oxidized at temperatures at around 230 °C, crosslinking occurs by oxidation, dehydrogenation, or both[12]. These fibers have to be pyrolyzed at temperatures above 1100 °C and must undergo a process called infusible stabilization, where the pitch is rendered infusible[1]. This and possible following heat-treatment procedures result in the formation of graphitic structures, the degree of which will affect the final microstructure, thermal, and mechanical properties.

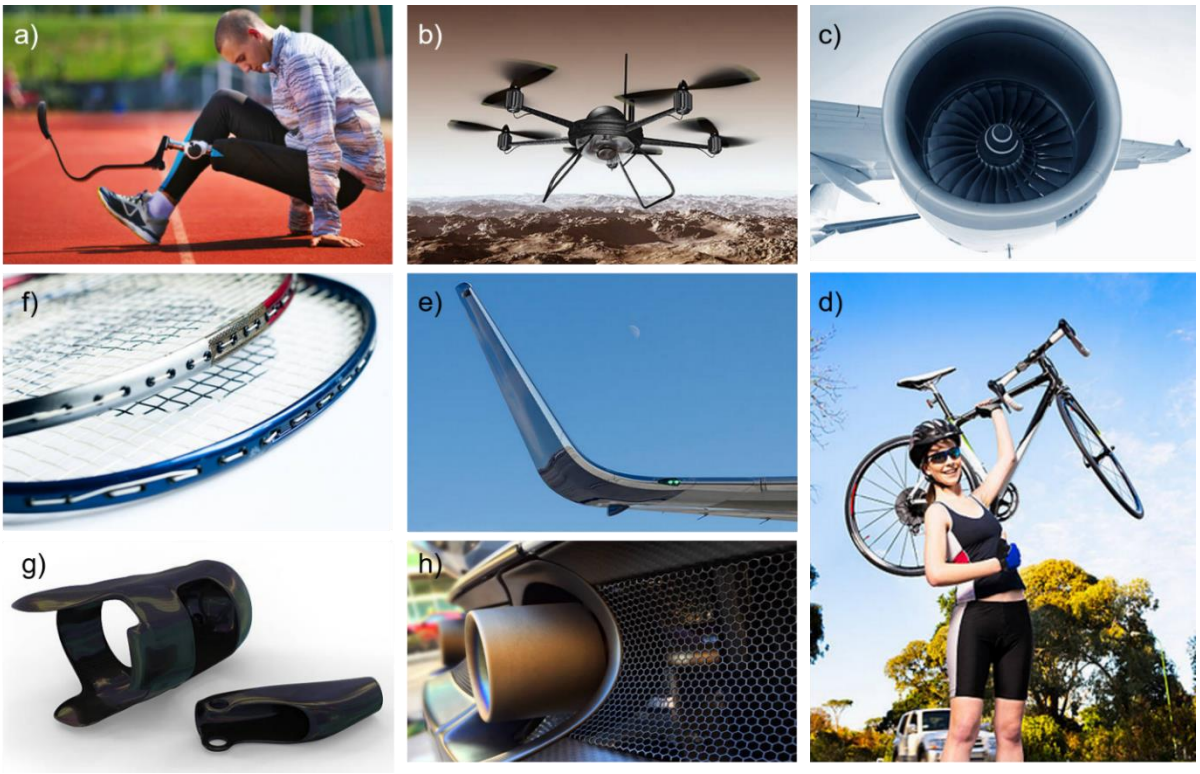

Figure 1. Carbon fiber applications of (a) prosthetics, (b) drones, (c) jet-engine-used turbine blades, (d) bikes, (e) winglets, (f) tennis racquets, (g) knee braces, and (h) car chassis [13].

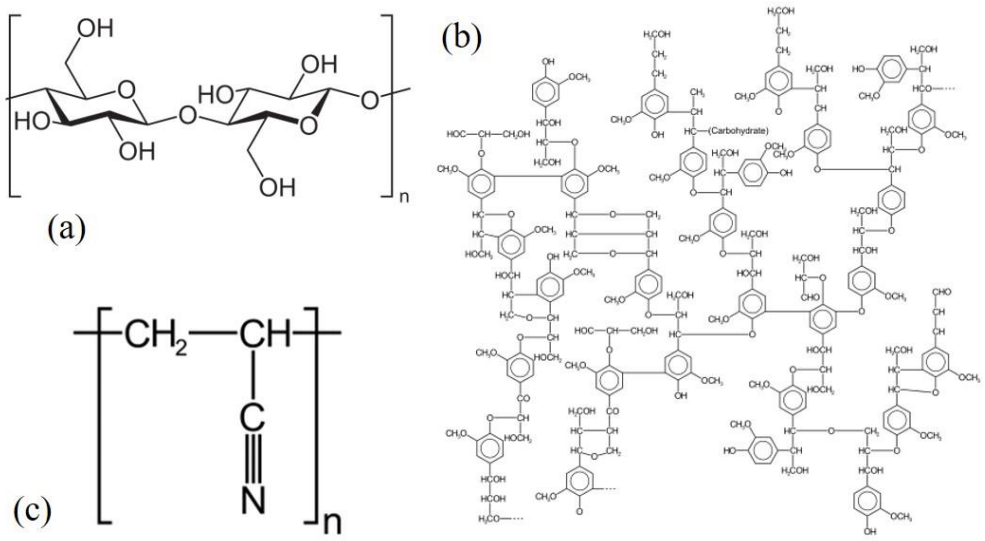

Figure 2. Molecular structure of carbon fiber precursors of (a) rayon composed of cellulose, (b) lignin, and (c) PAN[14].

1.1. Carbon fiber precursors – polyacrylonitrile (PAN)

Today over 90% of carbon fibers are PAN-based (**Figure 2c**). Due to the superior processability, thermal stability, and mechanical properties obtained in the resulting CFs upon pyrolysis, PAN has become the preferred precursor material for CF synthesis. The synthesis of PAN-based CFs begins with the polymerization, follows with fiber spinning, and ends with a series of heat-treatment at different temperatures. During fiber spinning, chemical and mechanical processes will be used to align the polymer macromolecules[15]. The pCFs should have the lowest possible diameter, maximum possible chain orientation, and high crystallinity[14]. Optimizing these properties in the precursor fiber will give the better-performance CFs after appropriate heat-treatment.

1.2. Carbon nanofillers for PAN reinforcement

To improve the mechanical (e.g., strength and modulus) and functional behaviors of PAN-based carbon fibers, reinforcement fillers have been incorporated into PAN during fiber spinning. The incorporation of reinforcement also enables the use of temperatures as low as 1200 °C for carbonization[16], eliminating the need for expensive high-temperature equipment. The nanoparticle concentration, alignment, and the interfacial interactions to PAN, as well as the physical properties of nanoparticles (e.g., sizes, aspect ratios, surface functional groups), will determine the reinforcement efficiency. More importantly, some nanoparticles, especially when their morphologies and orders can be well controlled, can initiate and modify polymer [17,18]. Specifically, the inclusion of nanoparticles with positional and orientational orders in PAN has been reported to develop a high degree of

crystals. As a result of this, specific nanofillers can induce the formation of aligned PAN molecules, ordered graphitic structures during carbonization and graphitization and thus higher performance[17]. The presence of reinforcement can potentially allow for more graphitization at relatively low carbonization temperatures[19]. A few general carbon nanoparticles frequently used in PAN-based polymers will be briefly introduced in the following sections (also listed in **Table 1**). The inclusion of nanoparticles has been efficient in enhancing the mechanical or functional properties. Usually, gel-spinning was used for mechanically durable carbon fibers, while electrospinning was used for energy and power applications (**Table 1**). In most cases, the inclusion of nanoparticles showed the improvement of mechanical properties after carbonization, but not necessarily upon oxidation. A careful look at the nanoparticles has shown a frequent use of nanocarbon, such as nanotubes or nanocrystals, instead of graphene-related powders. The reason can be due to the challenges in controlling graphene exfoliations and orientations. The following description of the particles will shed light on the nanoparticles used in reinforcing PAN polymers and their specific applications.

Carbon nanospheres (CNS): Carbon nanospheres or buckminsterfullerene is a hollow carbon sphere. It is mostly used to enhance the electrical properties of nanofibers by way of improving capacitance in the electrode and improving electrocatalytic activity[20]. Carbon nanospheres have been successfully incorporated on to the surface of fibers to improve the electrical performances for applications as electrodes and sensors[21] and electromagnetic shielding in aircraft and space-based systems[22].

Carbon Nanotubes (CNT): Carbon Nanotubes (CNTs) with their exceptional mechanical properties have been used as nanofiller reinforcements in carbon fibers and other composites. The mechanical properties of composites reinforced with CNT have been significantly improved depending on how well it has been dispersed in the matrix material without disrupting its integrity[23]. Researchers have also tapped into the electrical and thermally conductive nature of CNTs to impart similar properties to the CFs. However, obtaining a stable homogenous dispersion in several polymer matrices remains a challenge due to the concentration of CNT in the solution, length, entanglement of CNT and viscosity of the matrix[24].

Graphene-related materials:

Graphene Nanoplatelets (GNP): Graphene materials have impressive electrical, mechanical, and thermal properties. The high specific surface areas and a high aspect ratio[15,18,25,26]. These nanoparticles tend to be stacked through Vander Waal forces. Exfoliation of these nanoparticles through the interactions with the polymer chain will impart directional properties in a composite. GNP is a novel reinforcing nanofiller for carbon fibers. Zhou et al.[27] show a dramatic improvement in the mechanical properties of the PA6 polymer composite on the incorporation of functionalized graphene. The tensile strength was shown to increase by 2.4 times and Young's modulus by 132% when compared to the pure PA6 fiber. GNP has a 2D geometry, a high aspect ratio[18], and the ability to be used as a templating mechanism for alignment [18]. The interaction of the GNP

with the polymer in the 3-phase morphology during the drawing would enable its exfoliation by overcoming the Vander Waals forces. Ultimately a single layer thick GNP would help enhance the mechanical properties of the fiber[28].

Graphene Nanoribbons (GNRs): Graphene nanoribbons (GNR) have been incorporated into CFs to enhance graphitization and conductivity[29]. Finite termination of graphene produces a semi-one-dimensional structure with a zig-zag structure or armchair structure[30]. It can also be obtained by cutting an unzipping CNTs. Facile incorporation of GNRs in carbon nanofibers resulted in increased electrical conductivity, as demonstrated by Wang[23]. These fibers were used to support platinum nanoparticles for electrocatalytic applications.

Graphene oxide (GO): Liquid crystalline GO (LCGO) can form high modulus fibers by dry spinning. Salin et al. use PAN as the matrix incorporated with 0.5 wt% LCGO particles. The tensile strength was improved by 115% and Young's by 152% [31]. The SEM micrographs showed no voids or cracks in the drawn polymer fibers.

Table 1. List of PAN/nanoparticle composite fibers and their properties

#	PAN		Nanoparticles		Spinning Method	Mechanical		Carbon fiber treatment temperatures				Ref.
	Mw (Kg/mol)	Wt %	Type	Wt%		Modulus (GPa)	Strength (GPa)	Draw ratio	Stabilization (ºC)	Carbonization (ºC)	Graphitization (ºC)	
1	240	14.4	CNT	1	Gel	253	5.5	32.4	240 & 295	1300	NA	32
2	513	10.5	CNT	1	Gel	24.5±0.8	1.0±0.1	7.9	NA	NA	NA	33
3	513	10.5	CNT	0.1	Gel	21.7±0.9	1.0±0.1	7.9	NA	NA	NA	
4	513	10.5	CNT	1	Gel	21.5±0.9	1.0±0.1	7.9	NA	NA	NA	
5	513	10.5	CNT	0.4	Gel	342	3.2 ± 0.8	~13	310	1450	NA	34
6	513	10.5	CNT	0.1	Gel	318	2.0 ± 0.4	~13	310	1450	NA	
7	513	10.5	CNT	0.5	Gel	273	3.1 ± 0.8	~13	310	1450	NA	
8	453 / 964	10.5	CNT	0.4	Gel	342	3.2 ± 0.8	~13	310	1450	NA	
9	247	15	NA		Gel	17.8±0.8	0.7 ± 0.03	23	NA	NA	NA	35
10	247	15	CNC	1	Gel	16.5 ± 0.9	0.7 ± 0.07	23	NA	NA	NA	
11	247	15	CNC	5	Gel	18.8 ± 1.4	0.7 ± 0.06	23	NA	NA	NA	
12	247	15	CNC	10	Gel	19.9 ± 1.0	0.8 ± 0.08	23	NA	NA	NA	36
13	247	15	CNC	20	Gel	20.8 ± 0.8	0.8 ± 0.03	29	NA	NA	NA	
14	247	15	CNC	40	Gel	17.7 ± 1.0	0.7 ± 0.0	29	NA	NA	NA	
15	247	60	CNC	60	Gel	20.7 ± 2.6	0.8 ±0.1	10	265	NA	NA	37
16	1700	0.06	NA	0	Gel	16.5 ± 3.2	0.8 ± 0.1	NA	NA	NA	NA	38

17	1700	6.5	NA	0	Gel	361 ± 45	4.3 ± 1.0	NA	220-230	600-800	1000-1500	
18	247	15	Lignin	~31	Gel	229 ± 7	2.0±0.4	16	266-305	1000	NA	[39]
19	247	15	Lignin	~31	Gel	254 ± 7	1.9±0.2	18	266-305	1200	NA	
20	247	15	Lignin	~24	Gel	260 ± 5	2.1±0.3	18	266-305	1200	NA	
21	247	15	Lignin	~16	Gel	242 ± 25	0.9 ± 0.2	20	266-305	1300	NA	
22	513	9.5	NA	0	Gel	18.5 ± 1.1	0.9 ± 0.06	20	NA	NA	NA	[40]
23	513	9.5	BNNT	1	Gel	17.2 ± 0.6	0.8 ± 0.07	22	NA	NA	NA	
24	513	9.5	BNNT	5	Gel	17.2 ± 1.1	0.764 ± 0.93	12	NA	NA	NA	
25	513	9.5	NA	0	Gel	273 ± 5	1.7 ± 0.3	20	265 & 305	1300	NA	
26	513	9.5	BNNT	1	Gel	258 ± 9	2.0 ± 0.2	22	265 & 305	1300	NA	
27	513	9.5	BNNT	5	Gel	243 ± 3	1.5 ± 0.4	12	265 & 305	1300	NA	
28	150	8	Si	10	Electro	NA	NA	NA	280	700	NA	[41]
29	150	8	Ge	30	Electro	NA	NA	NA	280	700	NA	
30	150	8	Sn	50	Electro	NA	NA	NA	280	700	NA	
31	80	20	Lignin/ Grp	1	Electro	NA	NA	NA	225	900	NA	[42]
32	80	20	Lignin/ Grp	5	Electro	NA	NA	NA	225	900	NA	

Terminology: BNNT, boron nitride nanotubes; CNC, cellulose nanocrystals; CNT, carbon nanotubes; Grp, graphene.

1.3. Precursor fiber spinning

The following spinning techniques are categorized based on the tools used for spinning (e.g., air heating, coagulation, the electrical voltage application (**Figure 3**)) and the state of materials (e.g., melt, gel, solutions). The choice of the synthesis process is entirely dependent on the end-use of the fibers and their desired fiber properties.

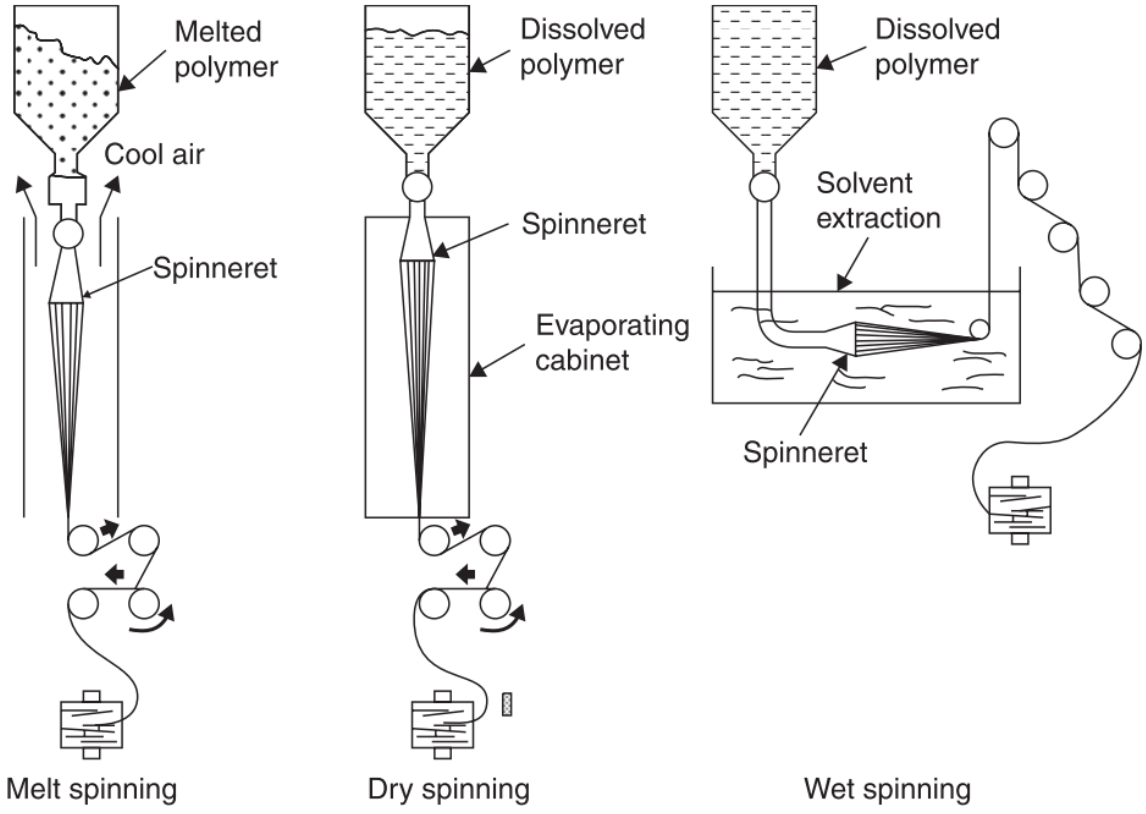

Figure 3. Schematics of melt, dry, and wet spinning[43].

Melt spinning: The polymer is heated and melted while the viscous melt is extruded through a spinneret into a cooling tube from which cold air is blown. The cool air allows for the solidification of the fiber from the melt[43]. The downside to this process is the presence of surface defects in the as-spun fibers. This can be mitigated by removing

impurities from the melt[14]. Melt spinning is used to spin fibers like Nylon 6,6. The mechanical properties of fibers fabricated through this technique is high, owing to the high degree of crystallization induced by the rapid cooling of the hot melt.

Dry spinning: This process involves introducing the spinning dope (i.e., a polymer dissolved in a volatile solvent as a polymer solution) into a heated chamber with a circulation of hot gases[14]. This method is specifically for those polymers that are susceptible to thermal degradation or cannot form thermally stable or viscous melts[43]. No coagulation bath is used. The dope is prepared by blending the polymer with additives and followed by filtration. It is then extruded into a spinning tube or evaporation chamber where the solvent is evaporated away. The fiber undergoes a chemical reduction in the heated chamber at high temperatures and dry fibers are obtained[44]. Stretching provides for the alignment of polymer chains along the fiber axis. Polymers spun by this method include PVC and acrylic.

Wet spinning: In this process, the polymer is dissolved into a solvent at a concentration with desired viscosity. It was first used to synthesize rayon fibers. Using a spinneret, the solution is extruded into a coagulation bath where they are partially stretched and solidified[43]. The spinneret is usually immersed in the coagulation bath and is primarily used to spin polymer fibers, which solidify gradually. The coagulant bath can be of water, glycerol, or acid. The diameter of the as-spun fiber depends on the diameter of the spinneret. The fibers are continuously wound up from the bath using take up drums[45].

Drawing is done to further align the polymer chains along the axial direction and to improve fiber properties[14]. Acrylic fibers are spun using this method.

Gel- or dry-jet wet-spinning: This prosses is similar to wet spinning, with the only difference being that the spinneret is placed a few centimeters above the coagulation bath (i.e., an air gap is present) (**Figure 4**). This method is used exclusively to spin polymer fibers that solidify from the melt instantaneously like PAN, PVA, and PS[18,43]. The presence of an air gap enables achieving higher orientations of the polymer chains when they are coagulated[7]. The fiber production speed for both wet and gel spinning is low compared to melt spinning[19,32,46,47].

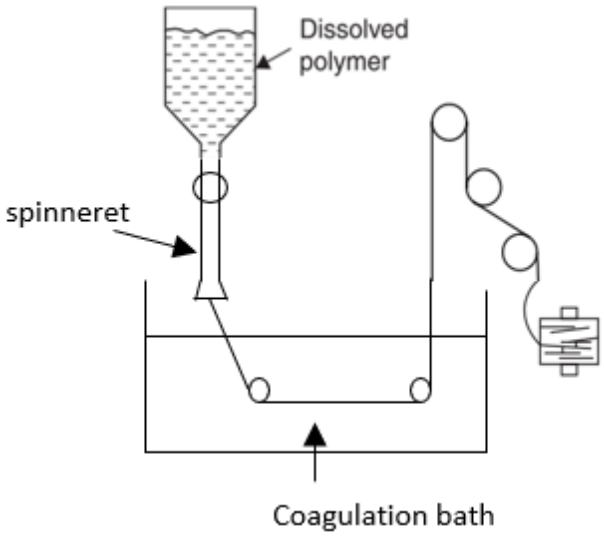

Figure 4. Dry-jet wet spinning setup.

Electrospinning: This process is governed by the electrohydrodynamic phenomenon where fluidic motioned is influenced by external and induced electric fields[48]. The high

electrostatic force applied on a polymer droplet distorts it into a conical form known as Taylor's cone once a critical voltage is achieved (**Figure 5**). The ejected polymer solution evaporates as it travels through the air, and fine nanofibers mats are deposited on the substrate[49]. This method is described in **Figure 5.** Fibers in the form of mats, yarns, tows, mats, and membranes can be obtained. The setup consists of a high voltage source, spinneret, and grounding. PAN fibers mats with a high specific surface area predominantly manufactured using this method. These surface of these fiber mats can be functionalized by incorporating particles like Si, Ge, and Sn for electrode applications[41].

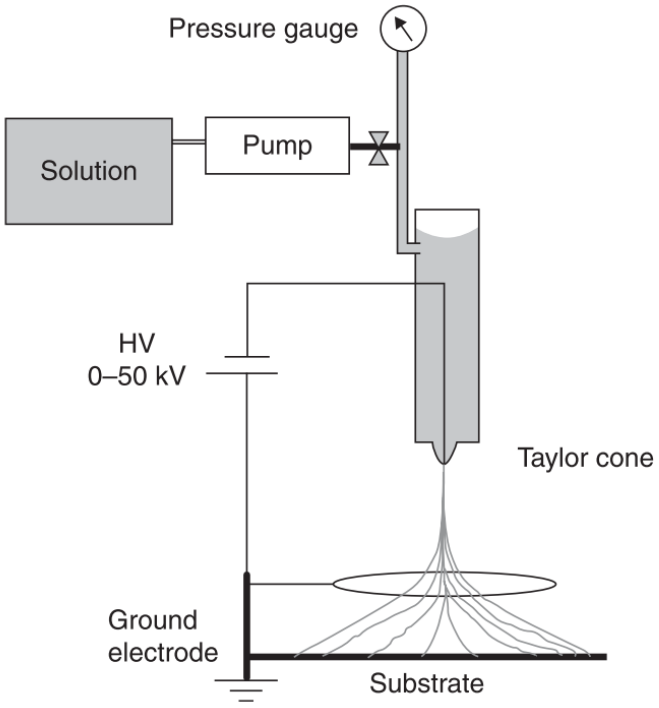

Figure 5. Setup of the electrospinning system [49].

1.4. Precursor heat treatment for carbon fibers (CFs)

Heat treatment of the precursor CFs is necessary for it to undergo necessary chemical and morphological changes to achieve the desired composition and structure. They are usually

performed in an ambient or inert atmosphere with or without tension dependent on the heating conditions (**Figure 6**). The fibers are treated in a tubular furnace with a heating rate of around 0.5 to 30 °C/min, with the lower heating rate providing the best mechanical properties[2,50–52].

Stabilization: It is an oxidative reaction at temperatures below 300° C with a heat treatment period ranging from 1 to 24 hours that breaks many of the hydrogen bonds and oxidizes the material[53]. At these low temperatures, the polymer chains loosen up and begin to flow around. The fibers are still ductile at this stage undergoes cyclization and formation of the planar ladder-like structures[54]. This initial heat treatment helps in dehydrogenation, aromatization, oxygenation, and crosslinking of the PAN polymer chains by breaking C≡N, creating C=N, and producing a conjugated ladder structure[51,55,56], a chemical change that prevents the fiber from melting at higher temperatures[51]. Dry air is usually the preferred atmosphere used within a furnace in which fibers under tension are placed. The properties of the fiber before heat treatment will have a massive impact on the properties of the fiber after heat treatment[7]; therefore, the as-spun fiber must be stabilized for the best quality. Care must be taken to control the extent of cyclization. Higher the cyclization would not necessarily translate to a better fiber[7,51]. In fact, studies have shown that excessive stabilization would lead to a skin-core structure[57]. Fitzer et al. determined through DSC measurements the optimal heating rate of copolymer methacrylate to be 5 °C/min for the initiation of the stabilization and later reduced to 1 °C/min to reduce overheating of the fiber[58].

Carbonization: PAN-based carbon fibers are carbonized in the temperature ranges between 700 – 1300 °C. Lower temperature ranges result in disordered carbon, and higher temperature treatments result in ordered hierarchical graphitic structures[19,51,59] that induce excellent mechanical properties in the fiber. This process is also to keep out non-carbon atoms (denitrogenation)[51]. The primary chemical reaction occurring in this stage of heat treatment is dehydrogenation.

Graphitization: Graphitization is the process of forming ordered hierarchical carbon structures. It is achieved at temperatures higher than 1300° C with the best graphitic structures obtained at above 2000 °C[60]. When heated in the right conditions, the chains bond side-by-side as ladder polymers and form narrow graphene sheets that merge to form a single, columnar filament. The orientation of the basal planes[51], resulting in the hierarchical graphitic structure and imparting excellent mechanical properties to the CFs, will also depend on the heating procedures. For example, CFs heated in the range of 1500–2000 °C (carbonization) exhibits the highest tensile strength (i.e., 5-6 GPa), while CFs heated from 2500 to 3000 °C (graphitization) exhibits a higher modulus of elasticity (i.e., 500-800 GPa)[61,62].

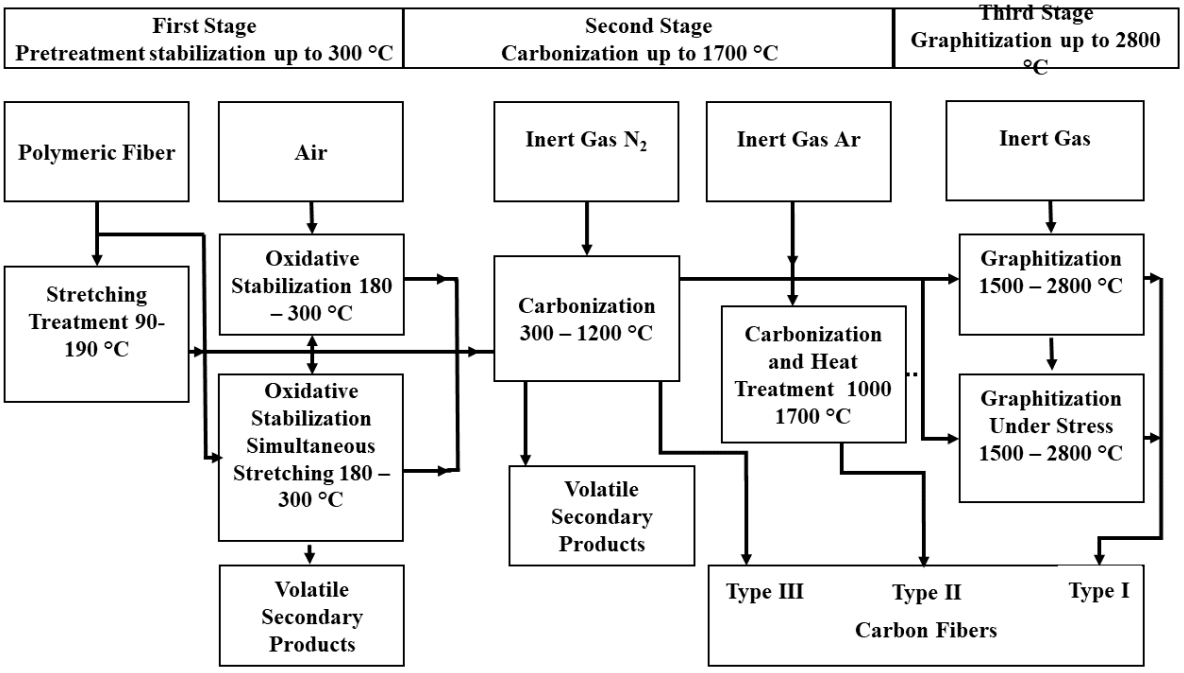

Figure 6. Process flow chart for the fabrication of carbon fibers

1.5. Fiber Morphology

Morphology of fibers achieved by using unique spinneret design allows the inclusion of multi-materials, manipulation of multi-structures, and control of functional at multiscale[18,47,63].

One-phase (1-phase) fibers:

- **Pure PAN:** This fiber morphology consists of pure polymer matrix **(Figure 7a)** material with no reinforcement. It is the simplest form of pCFs that can be manufactured. The mechanical properties of this fiber are dependent on the molecular weight distribution, copolymer content, and weight percentage of the polymer in the spinning dope, as well as the draw ratio during heat-treatment.

- **Porous fibers:** CFs with porous morphologies **(Figure 7b)** could be intercalated with ions and hence have applications in electrochemical energy storage[64]. Electrode applications for this fiber are immense. The hierarchical porous structures have a low resistance to ion movement and ultra-high capacitances. Due to the porosity, these fibers have high surface areas allowing them to be used as electric double-layer capacitors[65]. The porous CF can also serve as a catalyst (activated carbon) for electrochemical reactions[3,64,66] reducing the need for the use of expensive catalysts like platinum.

- **Hollow fibers:** Such morphology **(Figure 7c)** is desired in gas disposal, effluent disposal, desalination, energy storage due to their micropore structure, permeability selectivity, high absorption capacity[67]. One way of making such a fiber is by adding high boiling solvent lignin and alkaline lignin. During coagulation, the lignin delays the phase separation leading to the formation of hollow cores. When stored long enough in the coagulation bath, the porous regions coalesce into a hollow phase[63]. Hollow fiber morphologies could be used as drug delivery systems when the desired quantity of a drug could be released over time from a single capsule, electronics, 3-D printing, stimuli response are some of the other applications of such a fiber[67]. Zhang et al. have shown that hollow CFs have a porous inner wall. The mesopore ratio is around 17%, and the tensile strength and modulus were 3.37 and 85.82 cN/dTex[63].

Two-phase (2-phase) Fibers: Fibers with a particular templating/reinforcement phase **(Figure 7d),** which helps in the directional crystallization and alignment of polymer chains in the axial direction. This leads to an enhancement in the mechanical properties of the pCFs and subsequent improvements in the CFs after heat-treatment. The templating channel can be made of a polymer/reinforcement phase or just the reinforcement fillers. It must, however, be noted that the absence of polymer in the templating channel will lead to less adhesion between the phases and, therefore, lower mechanical properties[39,68].

- **Dispersed phase fibers:** CFs with reinforcement dispersed homogeneously **(Figure 7e)** within the polymer matrix are called D-phase CFs. The reinforcement helps improve the tensile strength and Young's modulus. The reinforcement material can be CNTs, graphene, metal nanoparticles, etc.[33,69,70]. Improved dispersion quality would promote efficient tress transfer from the polymer matrix to the reinforcement. Newcomb et al. demonstrated that with a better dispersion quality of CNT the interfacial shear strength could be improved by up to 40% [33].

- **Patterned fibers:** Such a fiber **(Figure 7f)** is manufactured by designing a flow path via the customization of the spinneret[2]. Intricate shapes of fiber cross-section can be achieved and these morphologies include the side-by-side, pie, and island-in-the-sea structures. Island-in-the-sea fibers are obtained by accommodating the spinning of two phases of the solution, one consisting of the PAN and the other a polymer phase like PMMA that will be burned off during the heat treatment process[47]. Another benefit to

this morphology is the ability to reduce the density of the carbon fiber without compromising the mechanical properties. Gulgunje et al. achieved densities as low as 0.9 g/cm^3 with a modulus of 209 N/tex[71]. The PAN phase could further be reinforced by particles of CNT, GNP, Grp, etc. like the D-phase fibers.

Three-phase (3-phase) Fibers: In many fibers, there can be a co-existence of three or even more phases composed of either distinct physical differences or chemical compositions (**Figure 7h**). A straightforward example will be the inclusion of more than two reinforcement fillers in the same polymer matrix to achieve the synergistic effects, including but not limited to the dispersion quality or the compliance of polymer chains on one-dimensional and two-dimensional fillers that is not easy to achieve for a single nanoparticle. Another example can be the inclusion of different polymers containing some specific nanoparticles for multifunctional properties. For example, Xu reported the one-step fabrication of polymer/nanoparticle/polymer three-phase (3-phase) fibers. Graphene nanoplatelets were used as a demonstration[18]. The benefit of the three-phase morphology is the exfoliation of the reinforcement GNP (in the middle layer) by the surface interactions between the polymer chains in the exterior and inner layer as during the drawing stage. This exfoliating action reduces the number of layers and the thickness of the GNP until a single layer thick GNP reinforcement channel is left. This would improve the mechanical properties of the pre-treated fibers due to improved alignment and crystallinity, and on further heat-treatment, it would help orient the graphitic planes in the axial direction hence, enhancing the mechanical properties of the carbon fiber.

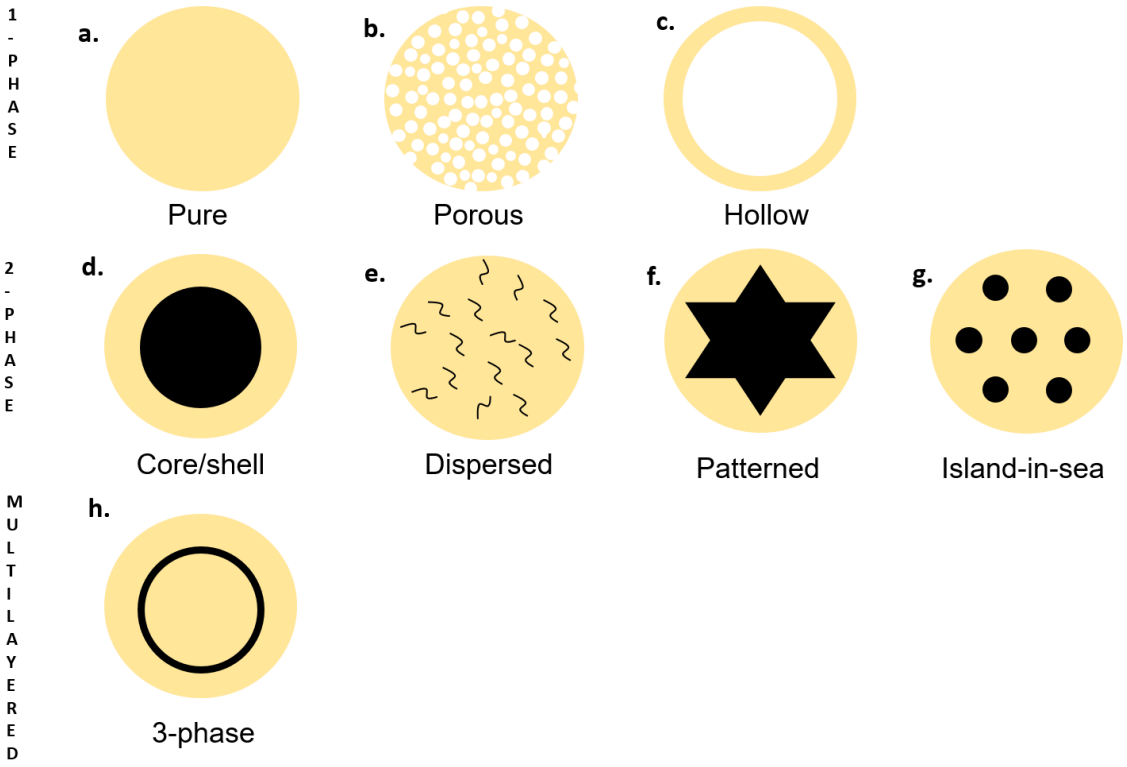

Figure 7. Different fiber morphologies are made possible with spinneret design.

Chapter 2. PAN Fiber Spinning and Characterizations

2.1. Materials

Polyacrylonitrile (PAN) (i.e., molecular weight 230,000 g/mol and mean particle size of 50 microns) copolymer (i.e., 99.5% acrylonitrile/ 0.5% methacrylate) was obtained from Goodfellow Cambridge Limited, England. N, N-Dimethylformamide (DMF) was obtained from Sigma-Aldrich, graphene nanoplatelets (i.e., surface area 750 m^2/g) was obtained from Sigma-Aldrich, carbon nanotubes (CNT) NC 7000 (i.e., avg. diameter 9.5 nm Avg. length 1.5 µm, avg. surface area 250-300 m^2/g) was obtained from Belgium Nanocyl SA, and, methanol for the coagulation bath was obtained from Sigma-Aldrich. All materials were purchased and used as obtained without further treatment.

2.2. Precursor fiber spinning

1-phase PAN fibers: A 15 wt% PAN solution was made by dissolving 22.5g of PAN in 150 ml of DMF. The concentration was so chosen as it provided the highest weight percentage of polymer that the syringe pump was able to extrude without getting jammed. The solution was placed on a hot plate maintained at 85 °C and stirred with the help of a mechanical stirrer at a low RPM for 2 hours to reduce the loss of solvent through evaporation. The end of the dissolution step is indicated by the formation of a golden liquid with a viscosity similar to that of honey. The solution was de-aerated in a furnace tube (Thermo Scientific Lindberg Blue M lab oven) maintained at a low vacuum for 1 hour. The spinning dope is then transferred to a metal syringe (80 ml capacity) and placed into the syringe pump setup (KD Scientific Legato 200) attached to a spinneret with the diameter

of 1 mm. The solution was spun into the methanol coagulant bath maintained at -50 °C and a separate one maintained at room temperature for comparisons. The air gap between the spinneret and bath was 2 cms. The solution was extruded at a rate of 2 ml/min where it undergoes solvent exchange and coagulates into a translucent fiber, which was taken up on to a reel at a high take-up rate. The fibers were kept immersed in the methanol bath overnight, dried and drawn over a hot plate in successive stages with incremental temperatures 110 °C, 130 °C and 150 °C, respectively. The total draw ratio was 6x. The fibers spun in room temperature methanol and -50 °C methanol, respectively, are named 15%PAN-RT and 15%PAN-50 fiber.

D-phase PAN-nanoparticle fibers: 15 wt% PAN solution was made by dissolving 22.5g of PAN in 150 ml DMF and heated on a hot plate maintained at 85 °C and stirred with a mechanical stirrer at a low RPM. A separate solution of 1g of GNP in 10 ml of DMF was obtained by tip sonication for 20 mins with a 5-sec pulse. The solution was de-aerated and spun into the methanol coagulant bath maintained at room temperature; the air gap was 2 cm. The as-spun fibers were kept immersed in the methanol bath and were dried and drawn the next day at temperatures of 110 °C, 130 °C, and 150 °C. The total draw ratio was 9x. This fiber is named 15%PAN/GNP-d. Because most literature reported an efficient reinforcement of carbon nanotubes in the PAN matrix, another same amount of CNT to GNP (e.g., 1g of CNT in 10 ml of DMF) was also added to the 22.5g of PAN/150 ml DMF solutions as a comparison.

3-phase PAN/PAN-nanoparticle/PAN fibers: 3-phase fibers as compared to the 1-phase and D-phase fibers were spun using a custom-made spinneret. The spinning set is shown in **Figure 8**. The spinneret has three channels corresponding to the exterior, middle and inner layers, with each of which being fed by one type of spinning dopes, leading to the blending or mixture of three phases coaxially distributed along the radial direction. For the inner and exterior layer, a PAN solution of 15 wt% was made by dissolving 22.5g of PAN in 150 ml DMF. The solution was heated on a hot plate maintained at 85 °C and stirred with a mechanical stirrer at low RPM. The composition of the middle layer was varied, according to **Table 2**. Weighted amounts of GNP and CNT were taken and dissolved in DMF, first by tip sonication 20 mins followed by a bath sonication of 2 hours until an optically homogeneous solution was obtained. Required amounts of the PAN were added, and the solution was placed on a hot plate maintained at 85 °C being stirred with a mechanical stirrer at a low RPM. The solutions were then de-aerated and transferred to three separate syringes fed for the core, sheath, and templating channels. A specially designed spinneret was used to get the desired morphology of the spun fibers. The dope was spun into the methanol coagulant bath at a rate of 1 ml/for the core and outer sheath and 2ml/min for the templating channel. The as-spun fibers were taken up on a reel at a high rate. The as-spun fibers were kept immersed in the methanol bath overnight and drawn the next day at consecutive temperatures of 110 °C, 130 °C and 150 °C. The total draw ratios are given in **Table 3**.

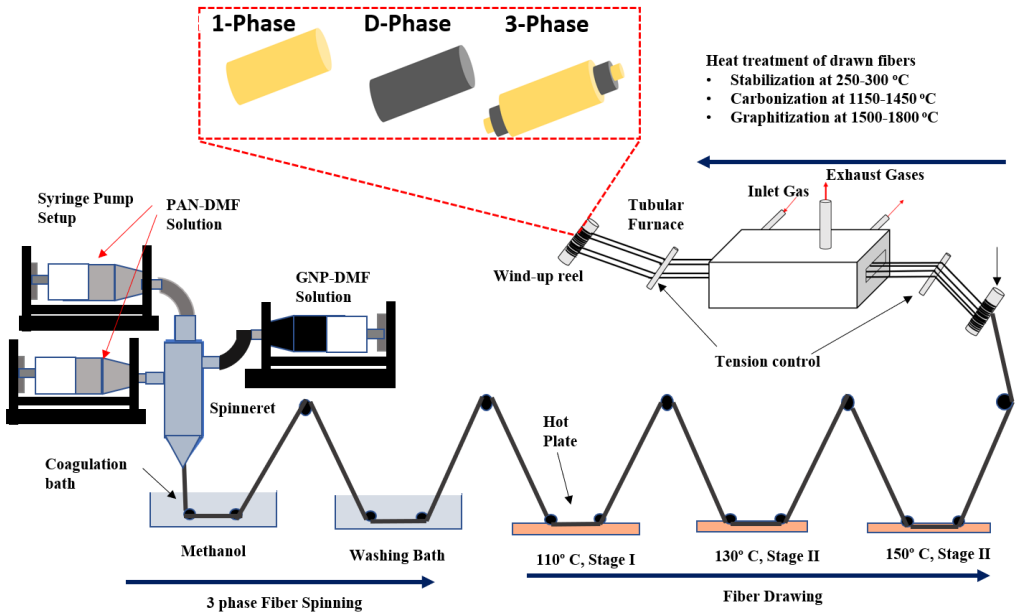

Figure 8. The fiber fabrication process, including the spinning, coagulation, drawing, and heat-treatment.

Table 2. Summary of as-synthesized fiber compositions

Number of phases	Fiber Name	Inner Layer	Exterior Layer	Middle Layer		
		Polymer content			Reinforcement Type	
		PAN wt %	PAN wt %	PAN wt %	GNP wt %	CNT wt %
1	15%PAN-RT	15		N/A	N/A	N/A
	15%PAN-50			N/A	N/A	N/A
D	15%PAN/GNP-D	15		N/A	1	N/A
3	0%PAN/10%GNP	15	15	0	10	0
	5%PAN/10%GNP	15	15	5	10	0
	10%PAN/10%GNP	15	15	10	10	0
	15%PAN/1%GNP	15	15	15	1	0
	15%PAN/1%CNT	15	15	15	0	1

2.3. Characterizations

Differential Scanning Calorimetry (DSC): DSC was conducted using a DSC 250 (TA Instruments Inc.). The sample weighing about 5 mg was placed on a titanium PAN and heated at a rate of 10 °C/min to 350 °C in a nitrogen atmosphere. The heat flow

characteristics and glass transition temperature were obtained. The thermal properties are summarized in **Table 3.**

Single Filament Tensile Test: Tensile tests were conducted using a Discovery HR-2 hybrid rheometer (TA Instruments Inc.). A constant linear strain rate of 150 µm/sec and a gauge length of 5 cm was used for the pre-heat-treated fibers, respectively. A number of 5-10 samples were tested for the average of the mechanical parameters.

Scanning Electron Microscopy (SEM): SEM images were obtained using a Philips XL-30 ESEM. Surface morphology data was observed, and data relating to the presence of voids and the adhesion between the phases were obtained, and the fiber topography was obtained.

Table 3. Summary of the mechanical properties of pre-treated polymer fibers

Number of phases	Fiber name	Draw Ratios				Thermal Properties		Mechanical Properties		
		110 °C	130 °C	150 °C	Total	T_g (°C)	Enthalpy (J/g)	Youngs modulus (GPa)	Tensile Strength (MPa)	Strain at break (%)
1	15%PAN-RT	1.6	2.5	2	8.0	88.3	473.9	9.34 ± 1.75	276.25 ± 43.75	8.1± 0.1
	15%PAN-50	2.4	2.5	2.7	16.2	74.1	466.9	8.76 ± 1.24	332.51 ± 27.58	27.0± 18.2
2	15%PAN/1wt%GNP-D	2.4	4	-	9.6	96.5	466.9	4.38 ± 0.80	188.26 ± 46.52	6.8± 6.2
3	0%PAN/10%GNP	1.4	1.9	2.5	6.7	71.4	220.9	1.28 ± 0.21	39.98 ± 4.91	8.4± 0.6
	5%PAN/10%GNP	3.4	3.4	-	11.6	57.4	287.2	4.49 ± 0.71	192.786 ± 26.35	10.2± 1.4
	10%PAN/10%GNP	**2.0**	**2.0**	**2.0**	**8.0**	**56.3**	**285.1**	**11.07 ± 0.87**	**418.373 ± 30.46**	8.2± 1.1
	15%PAN/1%GNP	2.3	2.3	2.3	12.2	78.9	292.8	9.01 ± 1.02	344.90 ± 24.85	9.4± 1.3
	15%PAN/1%CNT	5.3	2.3	2.3	28.0	48.7	310.8	9.76 ± 1.45	315.31 ± 41.35	9.6± 1.0

2.4. Results and discussions

Optimization of the PAN concentrations: Initially, the middle channel consisted of just GNP without any PAN mixture (i.e., GNP/DMF concentration of 10 wt%). Later, the GNP/DMF concentration was 10wt% while the PAN/DMF concentration increased in increments of 5 wt% from 0 wt% to 10 wt% (e.g., 10 wt% PAN/DMF with 10 wt% GNP/DMF meaning a GNP: PAN ratio of 1:1). Though there is an increasing trend for the mechanical properties as a function of the PAN:GNP ratio, this composition containing 10wt% GNP was unsuitable for the 3-phase fiber as the high concentration of GNP in the middle layer led to discontinuous GNP distributions during the spinning and drawing procedure. This is mainly due to the unmatched rheological behavior with the inner and outer PAN solutions. As the concentration of PAN/DMF in the middle channel was increased from 0% to 15%, a further improvement in tensile strength and Young's modulus was observed (**Table 3** and **Figure 9**). Though promising, the discontinuity of graphene in the middle layer made it challenging to process the composite fibers further.

It is worth mentioning that the interior and the exterior layers use a PAN concentration of 15 wt%. The spinning of fibers at the room temperature and -50 ^{o}C did not show too much difference for its mechanical properties (**Figure 10 and Table 3**). Therefore, for all experiments conducted in this paper, the room temperature condition was used for all fiber spinning. Also, notice that an attempt at fabricating a fiber with 15 wt% PAN and 10%

GNP in the middle channel composition was not possible as the rheology of such a solution provides a too high viscosity to spin fibers.

Since (i) 10 wt% nanoparticles, especially for the GNP, was too high for continuous fiber collection and post-treatment and (ii) 15 wt% PAN and 10 wt% GNP in the middle layer generated a too high viscosity for the fiber spinning, this study will start from a low concentration of GNP (1 wt%) at a PAN concentration of 15 wt% to demonstrate the nanoparticle reinforcement (**Figure 11**). At the same time, the interior and exterior layers also used the PAN/DMF 15 wt% dopes.

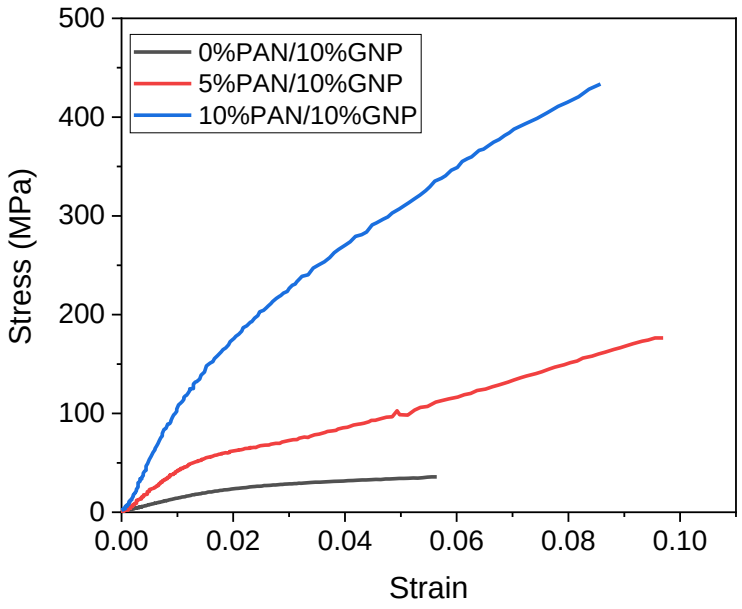

FIGURE 9. Single filament tensile tests of the 3-phase fibers with incremental PAN concentrations.

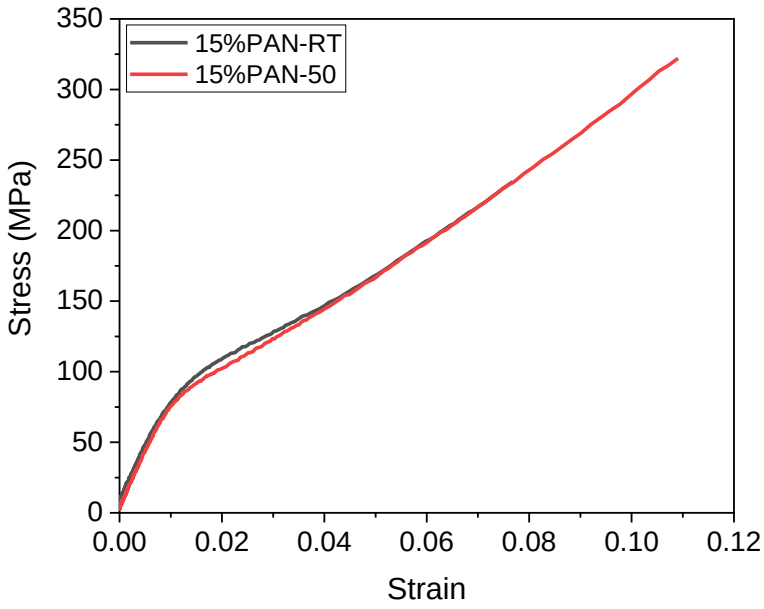

Figure 10. Single filament tensile test of 1-phase PAN fibers spun at room temperature (15%PAN-RT) and -50 ^{o}C (15%PAN-50).

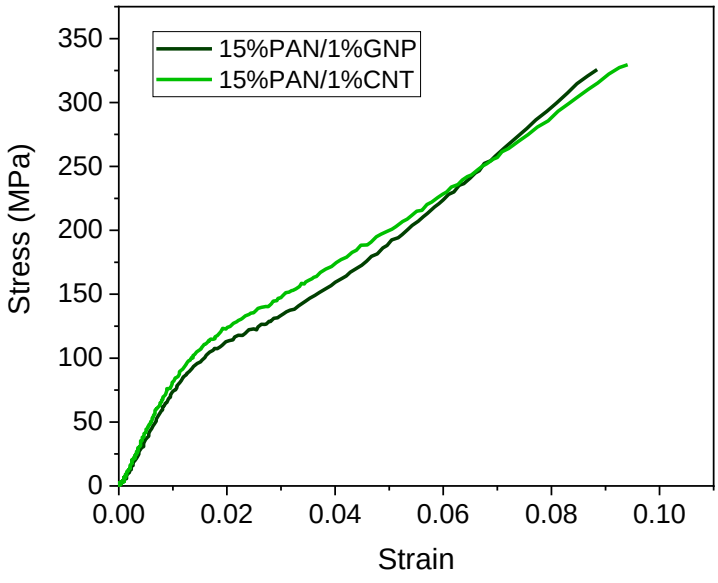

Figure 11. Single Filament tensile tests of 3-phase fibers with 1% GNP and 1% CNT in the middle channel.

The ratio of this specific content of PAN and GNP was also provided via an examination of the mechanical properties for the low ratios of PAN: GNP and their inefficient interactions. Fibers with no PAN content in the middle layer showed a phenomenon called slippage, as seen in **Figure 12**. This was in part due to the GNP acting a lubricant between the phases. When the tension was applied at the axial ends of this fiber, it would cause the exterior and middle layer to be displaced relative to each other. Upon failure, the sheath would fracture first, followed by the core at a later stage. This was seen to be hampering the mechanical properties of the fiber resulting in a less than desirable mechanical strength and Young's modulus. For this reason, the PAN/GNP ratios were increased to improve the middle layer interactions with the interior and exterior PAN channels. An increase of the PAN concentration to 15wt% for the interior and exterior layers and the simultaneous uses of 10 wt% GNP significantly increased the rheology, making the fiber non-spinnable.

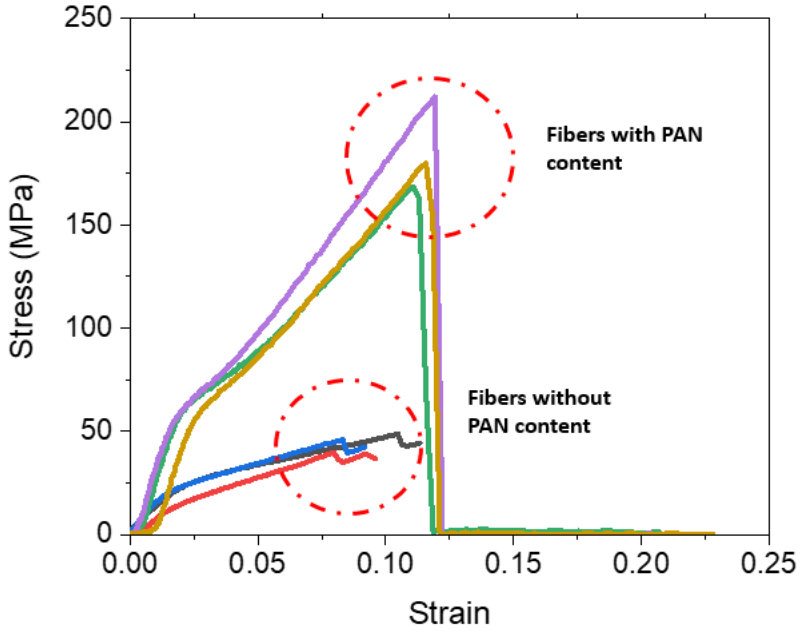

Figure 12. Effect of addition of 5 wt% PAN in the GNP middle layer on the fracture mode due to slippage.

Mechanical property comparison between the D-phase and the 3-phase fibers: Within the composites, the best mechanical properties were seen in the fiber with a 10wt%:10wt% composition of PAN: GNP in the middle channel. This is attributed to the improved adhesion between the phases in the pCFs. The D-phase samples, however, showed the least mechanical enhancement, possibly due to the dispersion quality and inefficient interfaces that are consistent with other literature reports. Attempts to spin simultaneously high concentrations of GNP reinforcement (i.e., 15 wt%) in the middle channel) was unsuccessful due to the high viscosity of the spinning solution. Thus, the 15% PAN with 1% nanoparticles (i.e., both GNP and CNT) were used to demonstrate their reinforcement

efficiently in mechanical properties (**Table 3**) and to study how these structures will further influence the mechanical performance of the carbonized fibers.

Chapter 3. PAN Fiber Carbonization and Characterization

3.1. Materials

The fibers synthesized in Chapter 2 and listed in **Table 3** were used in this section for carbonization to obtain carbon fibers and their subsequent characterizations.

3.2. Carbon fiber processing

Precursor fiber heat treatment for carbon fibers: The furnace used was a Thermo Scientific Lindberg Blue M 1700 box furnace. The schematic of the heat-treatment process is given in **Figure 11**. The fibers were wound around an alumina crucible boat so at to maintain tension during the process. The stabilization temperature was set to 280 °C with a heating rate of 5 °C/min and a hold time of 30 mins in the air followed by the carbonization at 1250 °C at a rate of 5 °C/min with a hold time of 10 mins in an ultra-high purity nitrogen atmosphere. The furnace was allowed to cool down to room temperature at 5 °C/min with constant nitrogen purging. The specific treatment procedures and the mechanical test feasibility are also listed in **Table 4**.

Table 4. Summary of the outcomes of the heat-treatment of fibers

Number of phases	Samples	The temperature of heat-treatment (°C)					Mechanical test feasibility
		Stabilization in air	Stabilization time (hrs)	Carbonization	Carbonization time (hrs)	Cooling time	
1	15%PAN-RT	**280**	**1.5**	**1250**	**4**	**4**	**Yes**
D	15%PAN/GNP-d						**No**
3	15%PAN/1%GNP						**Yes**
	15%PAN/1%CNT						**Yes**
	0%PAN/10%GNP						**No**
	5%PAN/10%GNP						**No**
	10%PAN/10%GNP						**No**

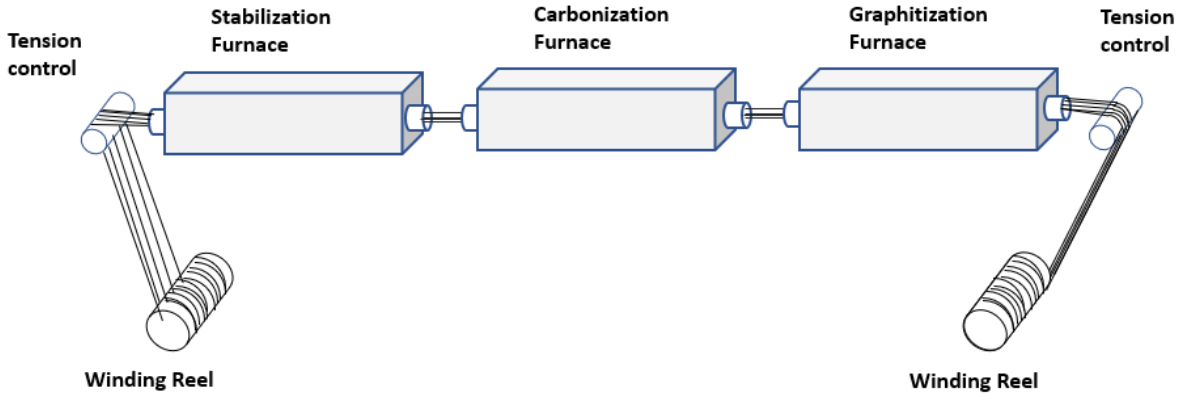

Figure 13. Heat-treatment setup.

3.3. Characterizations

Scanning Electron Microscopy (SEM): Scanning electron micrographs were obtained using a Philips XL-30 Environmental SEM. Surface morphology data was observed, and data relating to the presence of voids and the adhesion between the phases, topography of fracture surfaces were obtained.

Single Filament Tensile Test: Single filament tensile tests were conducted using a tensile tester (Discovery HR-2 hybrid rheometer). A constant linear strain rate of 50 μm/sec was used for the post-heat-treated carbon fibers. The low linear strain rate used to avoid premature fracture in the post-treated fibers as the fibers tend to be brittle in the lateral direction.

Electrical Resistivity Measurements: The resistivity measurements of the pre and post-heat-treated fibers were characterized using a multimeter (Keithley DMM 7510 digital) and the results were summarized as follows in **Table 6**.

3.4. Results and discussions

Morphology studies: Heat-treated fibers with optimized mechanical properties are summarized as follows. All fibers were carbonized at 1250 °C with the procedure mentioned in section 3.2. All the fibers that have been heat-treated (i.e., stabilized and carbonized based on the PAN and composite fibers from chapter 2) have the prefix HT- followed by the fiber name as given in chapter 2.

Thermal analysis of PAN: The PAN fibers were treated during the post-heat-treatment (i.e., stabilization and the carbonization stages). During pyrolysis from the TGA analysis, the polymer content shrinks significantly due to mass loss. Stabilization is done up to 280 °C in air. There is a significant mass loss in PAN, ~ 20% at ~300 °C (**Figure 14**).

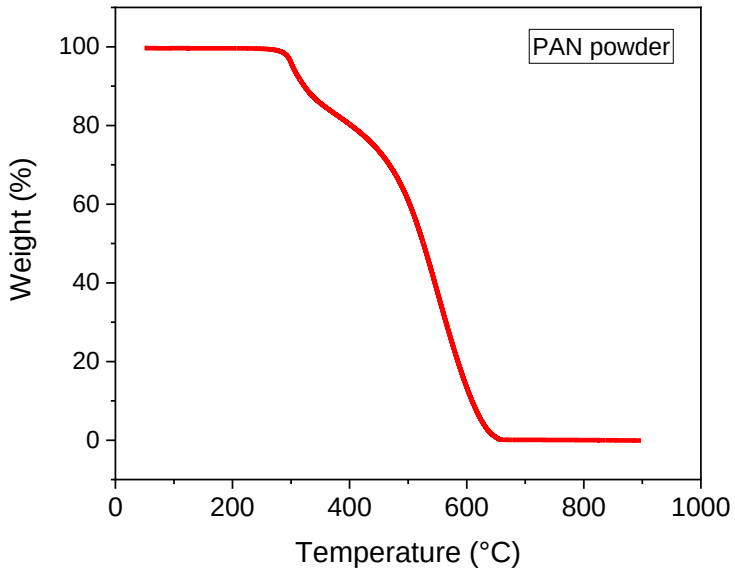

Figure 14. TGA of PAN. Note that mass loss begins at around 300 °C.

Morphology studies: The concentration of PAN in the middle layer was studied for its influence on the graphene morphologies, as shown in **Figures 15, Figure 16, and Figure 17**. **Figure 15** shows the morphologies of the 3-phase fiber with no PAN content in the middle channel both before (**Figures 15a-c**) and after (**Figures 15d-h**) the heat-treatment. The GNP materials were successfully separated from the interior and exterior PAN layers and distributed more loosely without strong bonding with the polymer layers that can be demonstrated by the fracture mode of delamination (i.e., the sheath peeling off from the core). The mechanical damage of this procedure may also reflect the sliding of the channels in slippage that can be observed in simple tension tests (**Figure 12**). Under mechanical tension, the middle layer tends to break first because of the voids trapped and the crack initiation, followed by the inner at a later stage. The GNP templating channel does not seem

to provide any mechanical benefits and is contributing to the deterioration of the mechanical properties. The heat-treatment did not enhance the packing of the graphene layers and retained the loosely distributed structures, with a high-resolution image showing the preferential alignment of these platelets. On the other hand, upon heat-treatment of the fiber, the polymer phases (i.e., interior and exterior layers) tend to shrink due to mass loss during the pyrolysis process while the GNP phase sees little to no mass loss or volume shrinkage. This led to a worse mechanical performance due to the more easily propagated cracks in the graphene layers because of a low-density phase sandwiched between two phases of higher packing densities.

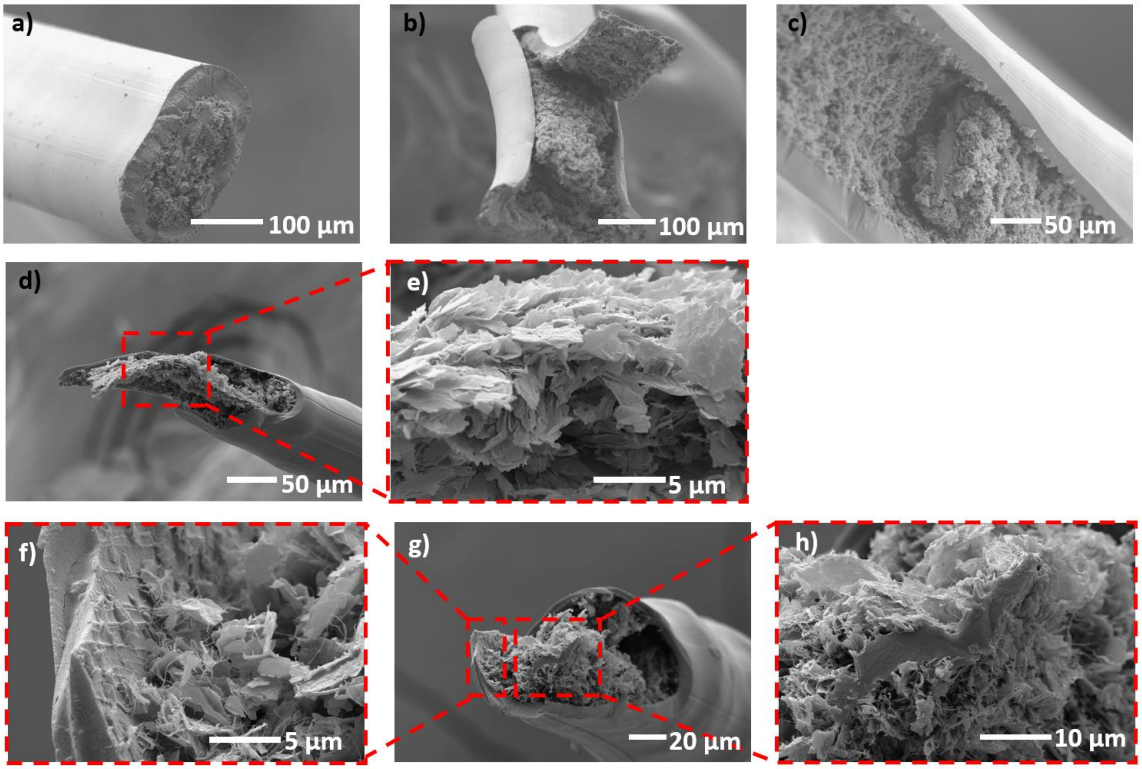

Figure 15. 3-phase fiber with the middle layer composition of 0%PAN/10%GNP. Pre-heat-treated fibers with morphologies of (a) cross-section; (b) exterior-middle layer interfaces; and (c) interior-middle layer interfaces. Post-heat-treated (i.e.,

stabilized and carbonized) fibers with morphologies of (d-h) fractured surfaces with loose but aligned GNP.

The effect of increased polymer content in the middle layer can be seen in **Figures 16** (i.e., 5wt% PAN/10wt% GNP) and **17** (i.e., 10wt% PAN/10wt% GNP). The orientation of the graphitic planes in the treated fibers have a high degree of alignment in the long axis direction. This is due to a combination of factors including better phase drawability and polymer filling among the graphitic planes, all leading to improved packing density. The microstructure that plays a crucial role in the mechanical properties of the fiber is significantly impacted by the PAN content in the templating channel. PAN has a marked effect on adhesion, drawability, density both before and after heat-treatment, and thus, the mechanical properties. The SEM micrographs show a trend where the previously mentioned properties are consistently improved with the addition of PAN in the templating channel. The concentration of PAN in the inner and exterior layers (i.e., 15 wt%) is higher than that in the templating channel (up to 10wt%). The difference in the concentrations leads to different shrinkage behavior when the fibers are pyrolyzed during heat-treatment.

Increasing the PAN content in the GNP channel contributes to greater alignment of the graphitic planes in the middle layers. This is attributed to the polymer aligning the GNP (**Figure 16**) during the three drawing stages. The final alignment in the axial direction translates to enhanced density and adhesion between the phases leading to better mechanical properties. On heat-treatment, the difference in shrinkage between the phases is similar though not equal as the PAN content in the templating channel (i.e., 5wt%) is

just one-third the PAN content in the core and sheath (i.e., 15 wt%). As a result, it has a marked improvement in mechanical properties (**Table 3** and **Figure 9**) as compared to the 3-phase fibers without PAN involvement in the middle layers. However, the adhesion between the phases is seen to be lacking (**Figure 14b and Figure 14c**). The GNP channel acts as a lubricant allowing slippage between the different phases, as seen in the mechanical test of this fiber (see single filament tensile test results for slippage in **Section 2.4 Figure 12**). **Figure 16** shows the effects of addition 5 wt% PAN in the middle layer. The alignment of the GNP is marginally improved on heat treatment (**Figure 16 a_1 and a_2**). **Figure 16 b_1 and b_2** show improved density, reduction in voids, and enhanced adhesion of the middle layer to the inner layer. A further increase of the PAN concentrations to 10w% (**Figure 17**) provided fiber spinning dopes with a 1:1 ratio of PAN to GNP in the middle channel, showing the best mechanical properties as expected (shown in **Table 3** and **Figure 9**). This is attributed to an improved higher density of the GNP, resulting in a low concentration of voids, the orientation of graphitic planes, more exceptional adhesion between phases, and continuity of the graphitic planes.

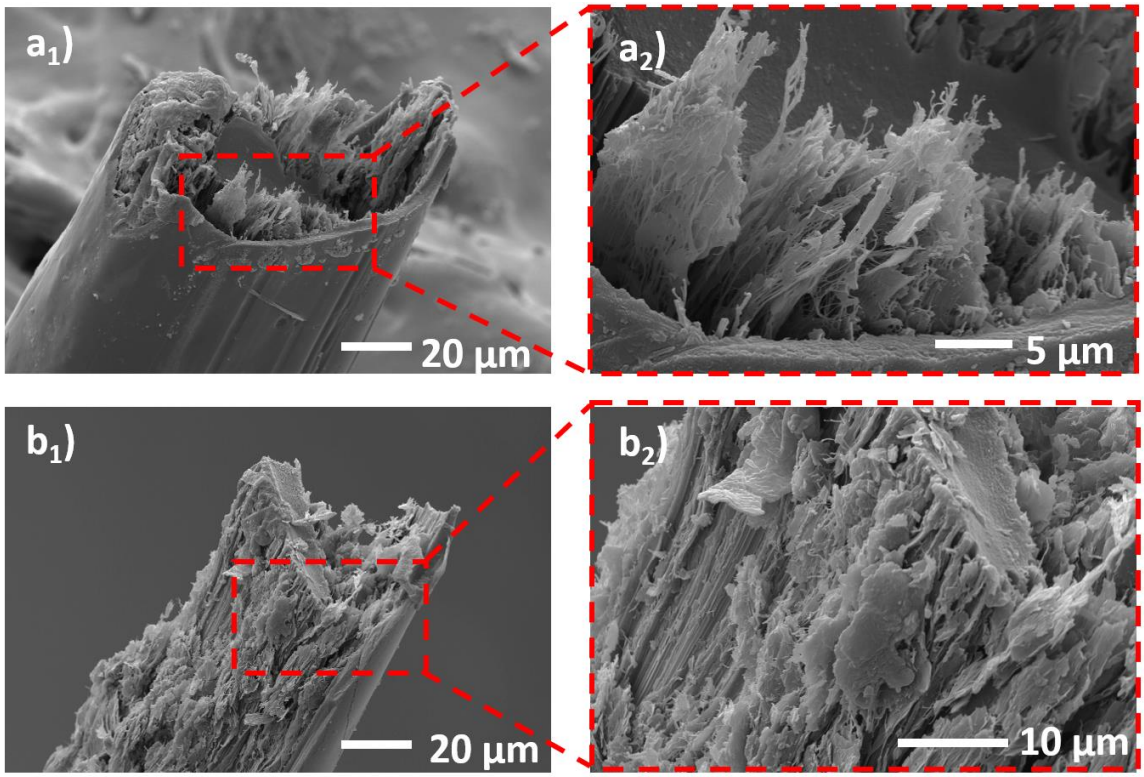

Figure 16. 3-phase fiber with the middle layer composition of 5%PAN/10%GNP with post-heat-treatment (e.g., HT-5%PAN/10%GNP). (a_1-a_2) middle-layer; (b_1-b_2) interior-middle interfaces; and (a_1-a_2) middle-exterior interfaces, all showing an increase of GNP alignment with higher GNP content in the middle layer but with loose structures and void presence.

A high degree of microstructural control was achieved when the PAN concentration was increased. This is seen when **Figure 15, Figure 16,** and **Figure 17** are compared. In **Figures 15** and **16** the adhesion between the different phases was poor in the pre-treated and the post-treated fibers leading to poor mechanical properties. **Figure 14** showed the best adhesion and orientation that was achieved, translating to better mechanical properties. The increase in the mechanical properties of the 3-phase fibers was due to the increase in PAN content in the middle channel. A decision was made to increase the polymer content further to 15 wt. % and reduce the nanoparticle content to 1 wt. %. This composition would

be similar to the compositions used to fabricate the one-phase fibers reported in several prior studies.

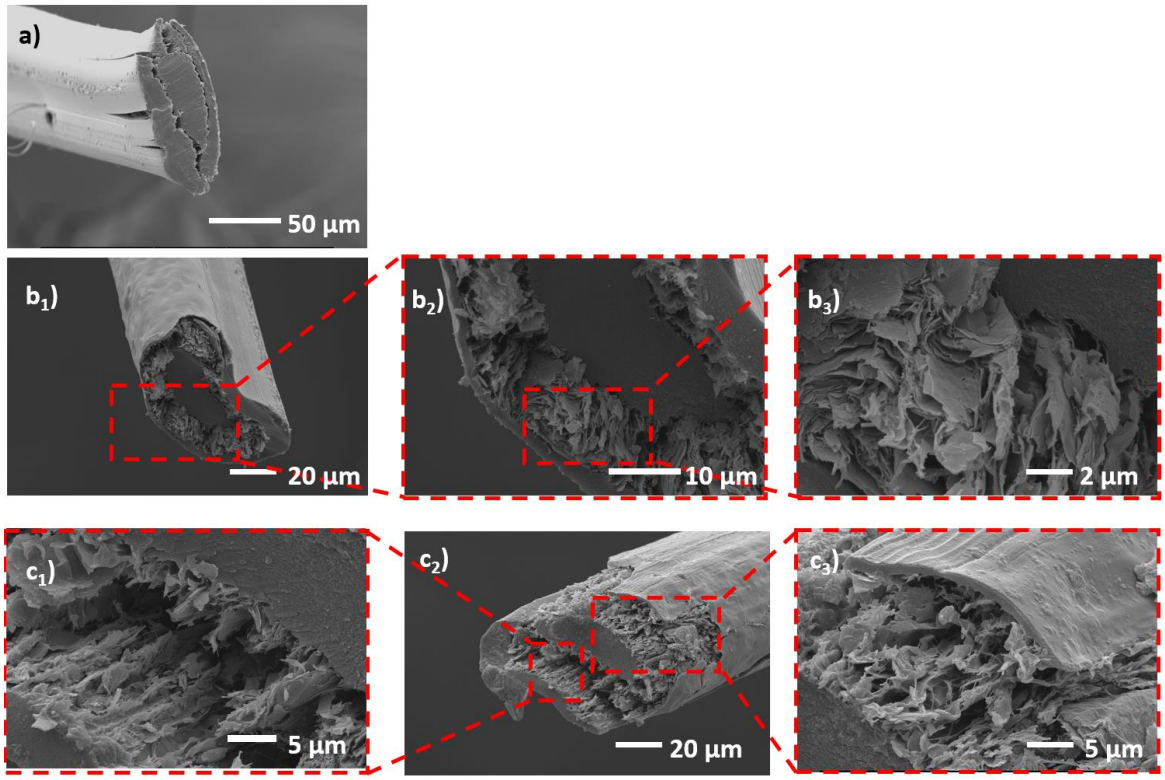

Figure 17. 3-phase fiber with the middle layer composition of 10%PAN/10%GNP with post-heat-treatment (e.g., HT-10%PAN/10%GNP). Morphologies of fiber fractured surfaces (a) before heat-treatment; (b_1-b_3) after heat-treatment with the interior-middle interfaces; (c_1-c_3) after heat-treatment with the exterior-middle interfaces.

Mechanical properties: 3-phase 15%PAN/1%GNP fibers exhibited the best mechanical properties after the heat-treatment (**Table 5**). We could attribute this to the high aspect ratio of the GNP reinforcement when compared to the CNT, leading to a better orientation and continuity in the graphitic planes over the CNT reinforced fiber and single-phase fiber. Mechanical properties of D-phase fibers (i.e., 15%PAN/GNP-D), and 3-phase fibers (i.e.,

the exterior and interior composition of 15 wt% PAN, and, the middle-layer compositions of 0%PAN/10%GNP, 5%PAN/10%GNP, and 10%PAN/10%GNP) were dismal before the heat-treatment (**Figure 3**), with the 15%PAN/GNP-D fiber not surviving the heat-treatment process on multiple occasions. The 3-phase fibers with different PAN concentrations (i.e., the middle-layer compositions of 0%PAN/10%GNP, 5%PAN/10%GNP, and 10%PAN/10%GNP) fibers did survive the heat-treatment process and also were too brittle (see mechanical feasibility **Table 4**) in the lateral direction preventing them from being clamped for mechanical characterization. **Figure 18** shows the stress-strain curves of the fibers that were mechanically feasible, and their properties are summarized in **Table 5**.

Table 5. Summary of heat-treated fibers

Fiber Name	Youngs Modulus (GPa)	Tensile strength (MPa)	Strain at failure (%)
HT-15%PAN-RT	42.3 ± 11.4	316.4 ± 107.6	1.5 ± 0.5
HT-15%PAN/1%GNP	74.6 ± 17.6	440.6 ± 145.9	1.3 ± 0.6
HT-15%PAN/1%CNT	38.9 ± 22.2	290.3 ± 137.3	1.1 ± 0.9

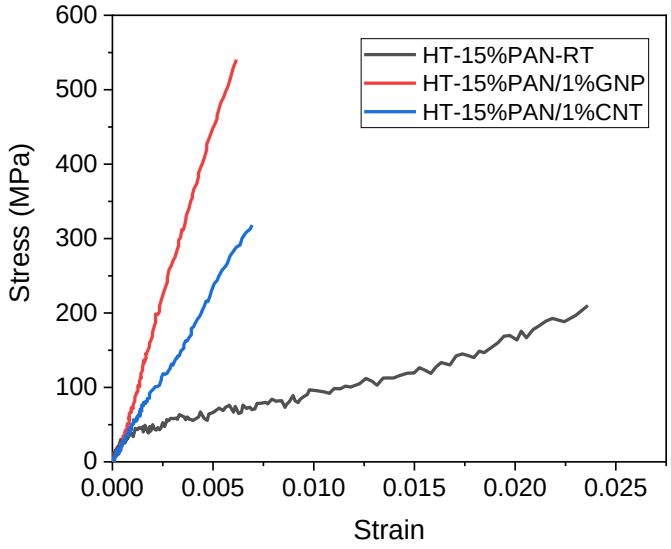

Figure 18. Single filament tensile test of heat-treated fibers.

Statistical Distribution for Tensile Strength: The Weibull modulus is used to statistically characterize the strength of materials based on the assumption that failure occurs at the most critical flaw [723238]. The Weibull statistics show the variability in mechanical properties in fibers due to the distribution of defects. It can be used to determine the structural viability of materials. Most fibers follow the Weibull model. The Weibull distribution is given by **Eq. 1** and **Eq. 2.**

$$\boldsymbol{P(\sigma) = 1 - \exp\left[-\left(\frac{\sigma}{x_o}\right)^{\beta}\right]} \qquad \textbf{Eq. 1}$$

$$\boldsymbol{ln\left(ln\frac{1}{1-P(\sigma)}\right) = \beta[ln\sigma - \ln(x_o)]} \qquad \textbf{Eq. 2}$$

A linear fit of the plot obtained from Eq.2 will give the shape parameter, β and scale parameter, x_o, σ is the failure strength. Probability of failure, $P(\sigma)$ is given by

$$P(\sigma) = \frac{i - 0.5}{N} \qquad \textbf{Eq. 3}$$

Where N is the number of samples and i is the failure rank. The Weibull modulus or shape parameter β, defines the variability of the distribution. A higher β is desired as it translates to a narrower distribution and a lower β means a broader distribution. Synthetic fibers have a Weibull modulus between 2 and 20. The Weibull modulus for each of the heat-treated fiber was fitted using the least square method summarized in **Table 6**. The x_o values predict the modulus and strength of the fiber when modulus and strength fitting is done. The x_o values of the modulus and strength are more predictive for the intrinsic mechanical properties of the fibers, considering their defects and showing great potential in further improving the fiber qualities.

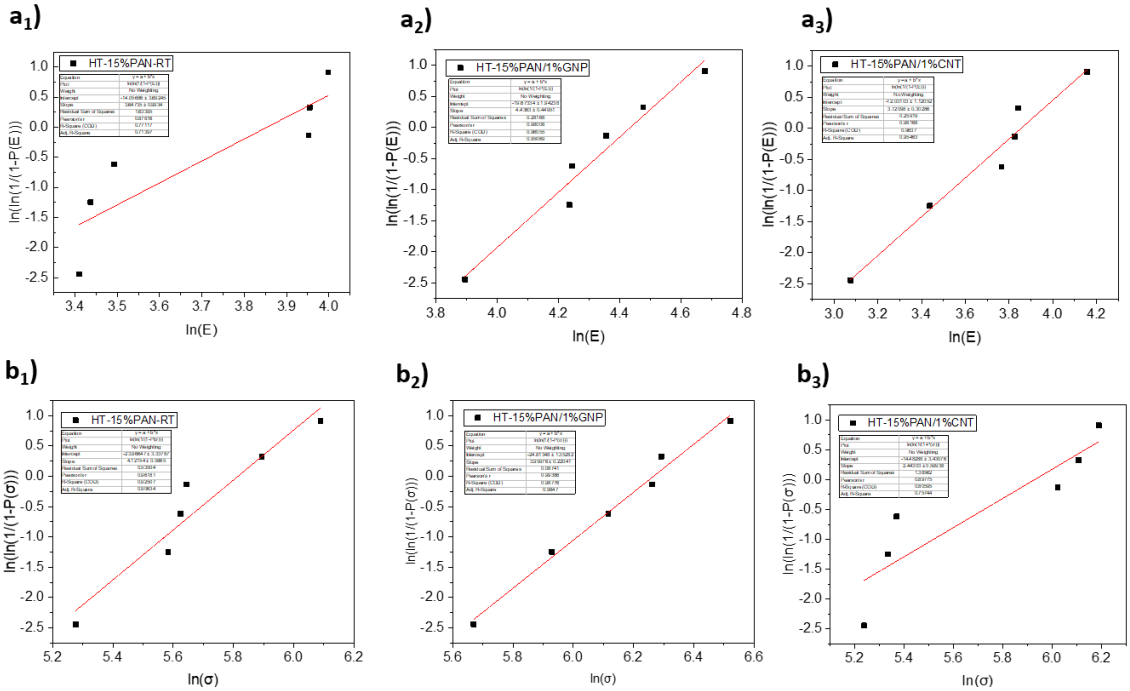

Figure 19. a_1, a_2, and a_3. Show the modulus fitting, while b_1, b_2, and b_3 show strength fitting of the various fibers summarized in **Table 6.**

Table 6. Weibull parameters of heat-treated fibers.

	Modulus fitting			Strength fitting		
Fiber Name	**Tensile modulus (GPa)**	**Scale parameter x_o (GPa)**	**Shape parameter, β**	**Tensile Strength (MPa)**	**Scale parameter x_o (MPa)**	**Shape parameter, β**
HT-15%PAN-RT	42.3 ± 11.4	47.2	3.1	316.4 ± 107.6	335.0	4.1
HT-15%PAN/1%GNP	74.6 ± 17.6	84.3	4.4	440.6 ± 145.9	526.4	3.9
HT-15%PAN/1%CNT	38.9 ± 22.2	47.2	3.1	290.3 ± 137.3	375.5	2.4

Electrical properties: The pre-heat-treated carbon fibers showed no conductivity (i.e., infinite resistance) (**Table 7**) when measured with the multimeter. This could be attributed to the discontinuity of the GNP/CNT channel within the pre-heat-treated fibers. On heat-treatment, however, the formation of continuous graphitic planes allows pathways for electrical current to flow with varying resistance, as seen with different fiber compositions. The fiber having no GNP/CNT channel showed the maximum resistance (i.e., lowest conductivity). The fibers with GNP/CNT channel showed considerably higher conductivity, making them much more suitable for sensing applications.

Table 7. Resistivity measurements

Fiber	Resistance measured (Ω)	Length (m)	Diameter (m)	Area (m^2)	Resistivity (ρ) (Ω·m)
15%PAN-RT	NA	4.62E-02	6.77E-05	3.60E-09	NA
HT-15%PAN-RT	1.49E+03	4.75E-02	5.18E-05	2.11E-09	6.59E-05
15%PAN/1%GNP	NA	4.50E-02	8.24E-05	5.33E-09	NA
HT-15%PAN/1%GNP	8.41E+02	4.82E-02	4.76E-05	1.78E-09	3.10E-05
15%PAN/1%CNT	NA	4.91E-02	1.87E-04	2.75E-08	NA
HT-15%PAN/1%CNT	6.61E+02	4.77E-02	4.64E-05	1.69E-09	2.34E-05

Volatile Organic Compounds (VOCs) Sensing: Testing for the volatile organic compound was carried out by testing for change in electrical response (resistance) when concentrations corresponding to 30 ppm, 60 ppm, and 120 ppm of methanol was passed over the sensor made of HT-15%PAN/1%GNP fiber mounted on a rigid substrate with conducting wires attached to its ends (**Figure 20**). The increase in resistance can be explained by the formation of surface bonds between the CF and the VOC that resulted in barriers to the flow of electrons on the surface of the fiber.

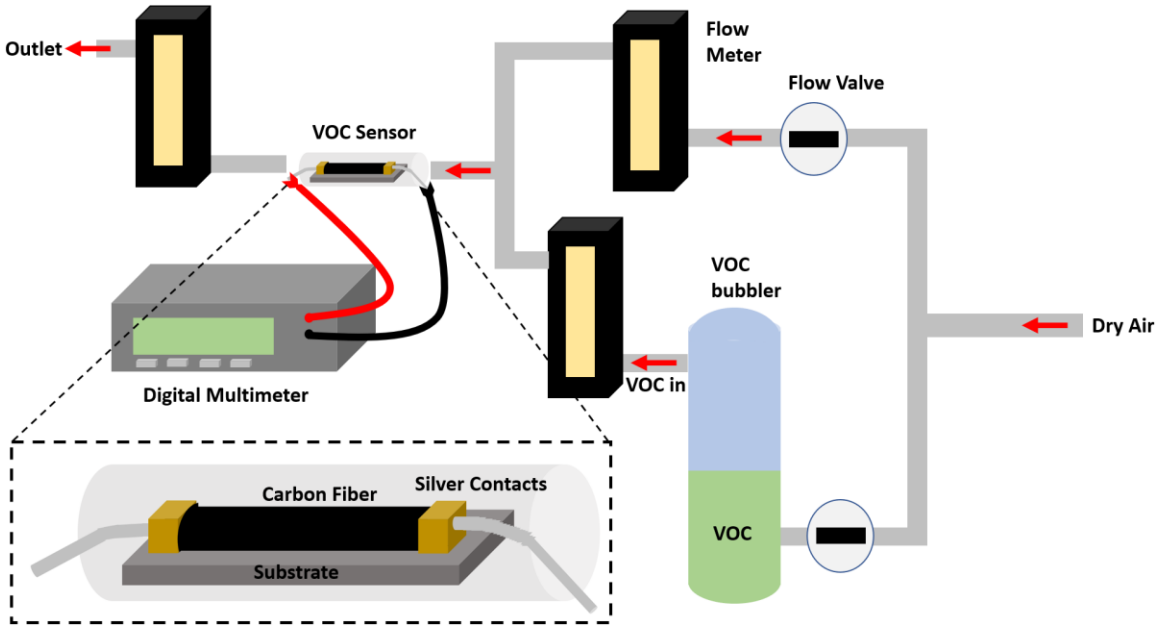

Figure 20. Carbon fiber VOC sensor and setup.

The ppm concentration was measured using the formula: $ppm\ conc. = \frac{W_0 - W_f}{t\ X\ total\ flow\ rate}$.

Where W_0 is the initial weight of the VOC, W_f is the final weight of VOC, and t is the time. The resistance was initially measured at t_0 corresponding to VOC flow diluted with air for 30 sec after which airflow was turned down to increase the concentration of VOC,

resulting in a change in resistance. The Airflow was turned up again after 30 sec to dilute the VOC concentration resulting in the resistance going back to the same base value. This was repeated for all three ppm concentrations summarized below in **Figure 21.**

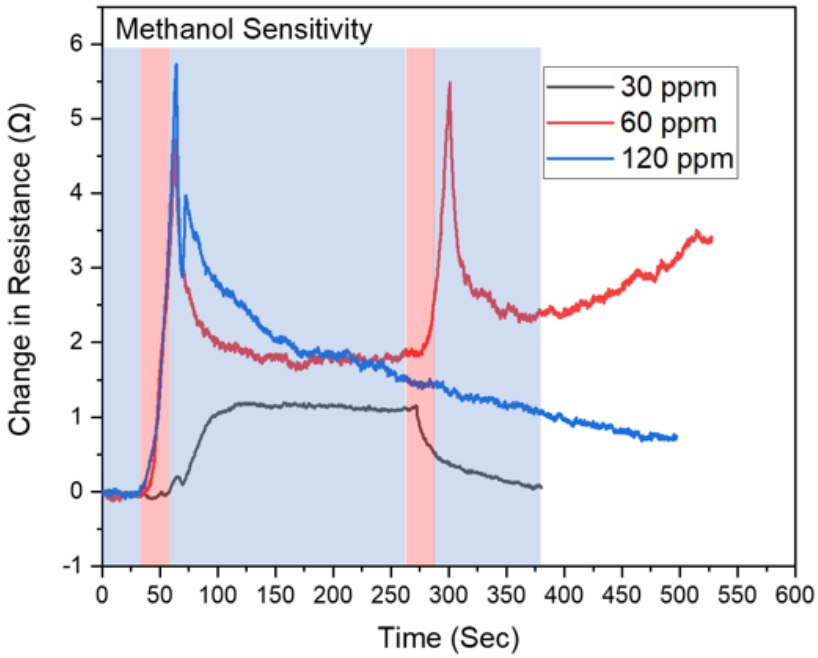

Figure 21. Methanol sensitivity. The blue shaded region indicates when the VOC and dry air was flowing through the sensor, and the red region indicates the point when the dry air was turned off.

The VOC sensor can detect organic compounds with concentrations as low as 30 ppm. At higher concentrations say 120 ppm, the sensor shows much latency in returning to base resistance. This can be attributed to the fact that the surface bonding is hard to break off at elevated concentrations resulting in a prolonged increase in resistance. For the moderately concentrated 60 ppm, the sensor shows a rapid spike in resistance when the airflow is stopped, followed by a rapid decline in resistance when the airflow is turned back up after 30 seconds. For the 30 ppm VOC concentration, the latency in recording the initial

resistance rise was higher than the first on/off cycle (i.e., higher than 60 seconds). The initial spike in resistance was recorded after several seconds after the dry air was turned back up after the first on/off cycle.

Pressure Sensing: A carbon fiber grid pressure sensor was fabricated using a 4-point mesh arrangement, as seen in **Figure 22.** This design was chosen as it would give the precise location of where the force was applied to the mesh pattern with high accuracy. The resolution of the sensor would be cogent on the density of the mesh network, with a higher mesh density translating to a better resolution. However, further studies are required in order to quantify the force applied accurately. It is observed that when pressure was applied at a node, which is a point of intersection between two carbon fibers (CFs), the measured resistance is reduced. This is because when the CFs, which are not insulated, contact each other on the application of pressure, it creates a new circuit allowing the current an additional pathway through which to flow. This is recorded as a drop in resistance on the multimeter giving us a precise location of where the force has been applied when two simultaneous measurements are taken. The resolution of this sensor was 10 mm as the fibers were arranged in a 10 mm x 10 mm grid. Lower resolutions are possible if the density of fiber within a square area is increased.

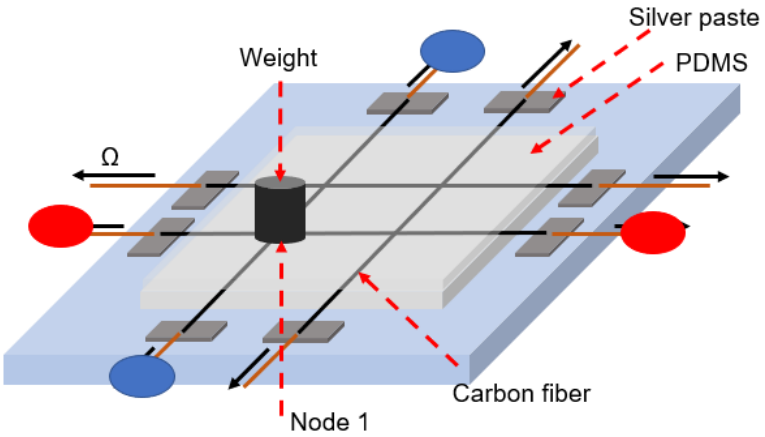

Figure 22. Schematic of the carbon fiber pressure sensor.

The two resistance measurements from the fibers connected at the blue and red terminals respectively were taken. This was done to ensure that both fibers at the intersection gave a response. This response is essential in determining the location of the applied pressure. The drop in resistance was seen at ~30 sec mark in both cases, and this was when the weight was applied, as seen in **Figure 23**. After a further 30 seconds, the weight was removed, resulting in a rise in resistance back to the base level. The resistance drops and take-offs were seen to be similar in onset and offset times, thus providing a proof of concept of this CF sensor. The green graph shows the response from the adjacent fibers. No observable drop in resistance was recorded. The features observed in the graph can be attributed to background noise.

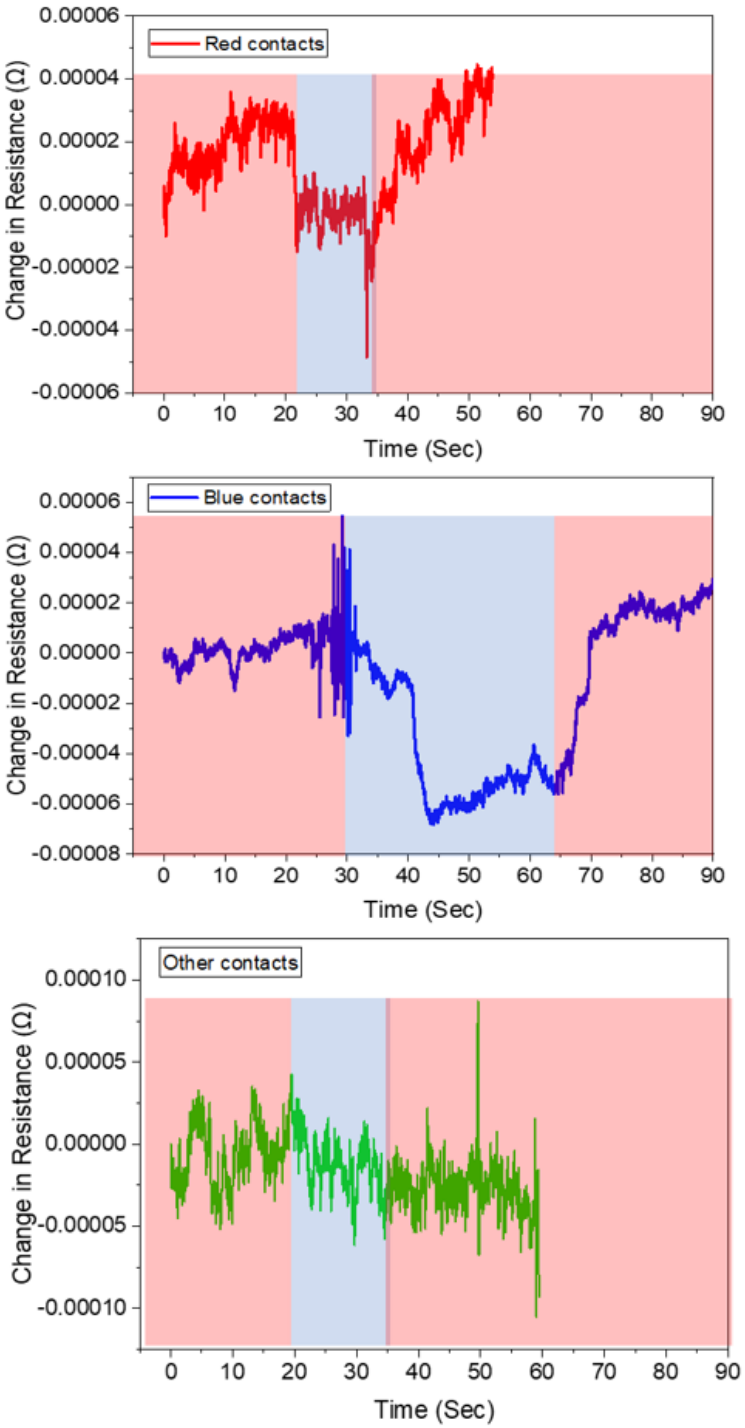

Figure 23. Resistance measurements of node 1. Blue and red graphs are indicating the measurements made from the blue and red contacts, respectively. The blue and red shaded region indicates the interval in which the force was applied and removed, respectively. The green graph shows the response from other contacts.

Chapter 4. Conclusions and Future Work

Mechanical properties of pCFs are dependent on the continuity, density, and interfacial action of the hierarchical graphitic structures. The presence of voids formed during crystallization due to the random dispersion of reinforcement/nanofiller in pre-carbon fibers (pCFs) deteriorates these properties. In this project, a specialized templating graphene channel was developed via a spinneret designed in house. This channel runs in the axial direction of the fiber and concentrically to the outer and inner polyacrylonitrile (PAN) channels. This channel is composed of graphene nanoplatelets (GNP) and a varying concentration of PAN. On drawing the as-spun fibers, the GNP is aligned in the axial direction. This channel then allows for crystallization along the axial direction and minimizes the formation of voids leading to enhanced mechanical properties. The mechanical test shows the composite as-spun fiber with GNP templating channel has improved modulus and tensile strength as compared to the pure PAN fiber, due to the alignment of the GNP. Resistivity, VOC sensitivity, and pressure sensitivity measurements were demonstrated as well.

For future work, a novel fiber morphology of “island-in-the-sea” microstructure should be examined due to the better control of PAN/GNP microstructures. This kind of morphology could be used to synthesize near-nano scale pre-carbon fibers. On heat treatment, the fibers will shrink to the nanoscale range of diameters. For the VOC sensor, an alternate arrangement of multiple fibers arranged in a series of rows or made to form a grid to

improve the sensitivity of the sensor could be attempted. The pressure sensor with a higher mesh density could be fabricated to improve the current 10 mm resolution to the micro and possible nanoscale resolutions. This can have applications in MEMS devices.

REFERENCES

(1) Chung, D. D. L. *Carbon Fiber Composites*; 2012. https://doi.org/10.1016/C2009-0-26078-8.

(2) Liu, Y.; Kumar, S. Recent Progress in Fabrication , Structure , and Properties of Carbon Fibers. **2012**, 234–258. https://doi.org/10.1080/15583724.2012.705410.

(3) Jost, K.; Stenger, D.; Perez, C. R.; McDonough, J. K.; Lian, K.; Gogotsi, Y.; Dion, G. Knitted and Screen Printed Carbon-Fiber Supercapacitors for Applications in Wearable Electronics. *Energy Environ. Sci.* **2013**, *6* (9), 2698–2705. https://doi.org/10.1039/c3ee40515j.

(4) Kim, H.; Jalili, R.; Spinks, G. M.; Wallace, G. G.; Kim, S. J. High-Strength Graphene and Polyacrylonitrile Composite Fiber Enhanced by Surface Coating with Polydopamine. *Compos. Sci. Technol.* **2017**, *149*, 280–285. https://doi.org/10.1016/j.compscitech.2017.05.029.

(5) MInus, M., Kumar, S. The processing, properties, and structure of carbon fibers. *JOM* **57,** 52–58 (2005). https://doi.org/10.1007/s11837-005-0217-8

(6) Jean-Baptiste Donnet - Carbon Fibers-Marcel Dekker (1998).

(7) Frank, E.; Hermanutz, F.; Buchmeiser, M. R. Carbon Fibers : Precursors , Manufacturing , and Properties. 493–501. https://doi.org/10.1002/mame.201100406.

(8) Hosseinaei, O.; Harper, D. P.; Bozell, J. J.; Rials, T. G. Role of Physicochemical Structure of Organosolv Hardwood and Herbaceous Lignins on Carbon Fiber Performance. **2016**. https://doi.org/10.1021/acssuschemeng.6b01828.

(9) Kizzire, D. G.; Rios, O.; Keffer, D. J.; García-negr, V.; Harper, D. P. Elucidating Nano and Meso-Structures of Lignin Carbon Composites : A Comprehensive Study of Feedstock and Temperature Dependence. **2020**, *161*, 856–869. https://doi.org/10.1016/j.carbon.2020.02.010.

(10) Kubo, S.; Kadla, J. F. Lignin-Based Carbon Fibers: Effect of Synthetic Polymer Blending on Fiber Properties. *J. Polym. Environ.* **2005**, *13* (2), 97–105. https://doi.org/10.1007/s10924-005-2941-0.

(11) Kadla, J. F.; Kubo, S.; Venditti, R. A.; Gilbert, R. D.; Compere, A. L.; Griffith, W. Lignin-Based Carbon Fibers for Composite Fiber Applications. *Carbon N. Y.* **2002**, *40* (15), 2913–2920. https://doi.org/10.1016/S0008-6223(02)00248-8.

(12) Guigon, M.; Oberlin, A. Preliminary Studies of Mesophase-Pitch-Based Carbon Fibres: Structure and Microtexture. **1986**, *25*, 231–241.

(13) https://www.istockphoto.com/photos/carbon-fiber

(14) Donnet, J. B., Bansal, R. C. *Carbon Fibers*; 1383.

(15) Mack, B. J. J.; Viculis, L. M.; Ali, A.; Luoh, R.; Yang, G.; Hahn, H. T.; Ko, F. K.; Kaner, R. B. Graphite Nanoplatelet Reinforcement of Electrospun Polyacrylonitrile Nanofibers **. **2013**, No. 1, 77–80. https://doi.org/10.1002/adma.200400133.

(16) Jiang, E.; Maghe, M.; Zohdi, N.; Amiralian, N.; Naebe, M.; Laycock, B.; Fox, B. L.; Martin, D. J.; Annamalai, P. K. Influence of Different Nanocellulose Additives on Processing and Performance of PAN-Based Carbon Fibers. *ACS Omega* **2019**, *4* (6), 9720–9730. https://doi.org/10.1021/acsomega.9b00266.

(17) Saha, B.; Dzenis, Y.; Schatz, G. C. Multi-Step Mechanism of Carbonization in Templated Polyacrylonitrile Derived Fibers : ReaxFF Model Uncovers Origins of Graphite Alignment. *Carbon N. Y.* **2015**, *94*, 694–704. https://doi.org/10.1016/j.carbon.2015.07.048.

(18) Xu, W.; Jambhulkar, S.; Verma, R.; Franklin, R.; Ravichandran, D.; Song, K. In Situ Alignment of Graphene Nanoplatelets in Poly(Vinyl Alcohol) Nanocomposite Fibers with Controlled Stepwise Interfacial Exfoliation. *Nanoscale Adv.* **2019**, *1* (7), 2510–2517. https://doi.org/10.1039/c9na00191c.

(19) Chae, H. G.; Minus, M. L.; Rasheed, A.; Kumar, S. Stabilization and Carbonization of Gel Spun Polyacrylonitrile / Single Wall Carbon Nanotube Composite Fibers. **2007**, *48*, 3781–3789. https://doi.org/10.1016/j.polymer.2007.04.072.

(20) Wu, L.; Shen, Y.; Yu, L.; Xi, J.; Qiu, X. Nano Energy Boosting Vanadium Fl Ow Battery Performance by Nitrogen-Doped Carbon Nanospheres Electrocatalyst. *Nano Energy* **2016**, *28*, 19–28. https://doi.org/10.1016/j.nanoen.2016.08.025.

(21) Tang, K.; Fu, L.; White, R. J.; Yu, L.; Titirici, M.; Antonietti, M.; Maier, J. Hollow Carbon Nanospheres with Superior Rate Capability for Sodium-Based Batteries. **2012**, 873–877. https://doi.org/10.1002/aenm.201100691.

(22) Zhou, C.; Geng, S.; Xu, X.; Wang, T.; Zhang, L.; Tian, X.; Yang, F.; Yang, H.; Li, Y. Lightweight Hollow Carbon Nanospheres with Tunable Sizes towards Enhancement in Microwave Absorption. *Carbon N. Y.* **2016**, *108*, 234–241. https://doi.org/10.1016/j.carbon.2016.07.015.

(23) Godara, A.; Mezzo, L.; Luizi, F.; Warrier, A.; Lomov, S. V.; van Vuure, A. W.; Gorbatikh, L.; Moldenaers, P.; Verpoest, I. Influence of Carbon Nanotube Reinforcement on the Processing and the Mechanical Behaviour of Carbon Fiber/Epoxy Composites. *Carbon N. Y.* **2009**, *47* (12), 2914–2923. https://doi.org/10.1016/j.carbon.2009.06.039.

(24) Ma, P.; Siddiqui, N. A.; Marom, G.; Kim, J. Composites : Part A Dispersion and Functionalization of Carbon Nanotubes for Polymer-Based Nanocomposites : A Review. *Compos. Part A* **2010**, *41* (10), 1345–1367. https://doi.org/10.1016/j.compositesa.2010.07.003.

(25) Li, D.; Müller, M. B.; Gilje, S.; Kaner, R. B.; Wallace, G. G. Processable Aqueous Dispersions of Graphene Nanosheets. *Nat. Nanotechnol.* **2008**, *3* (2), 101–105. https://doi.org/10.1038/nnano.2007.451.

(26) Ji, X.; Xu, Y.; Zhang, W.; Cui, L.; Liu, J. Composites : Part A Review of Functionalization , Structure and Properties of Graphene / Polymer Composite Fibers. *Compos. PART A* **2016**, *87*, 29–45. https://doi.org/10.1016/j.compositesa.2016.04.011.

(27) Zhou, L.; Liu, H.; Zhang, X. Graphene and Carbon Nanotubes for the Synergistic Reinforcement of Polyamide 6 Fibers. **2015**, 2797–2805. https://doi.org/10.1007/s10853-015-8837-z.

(28) Persson, H.; Yao, Y.; Klement, U.; Rychwalski, R. W. A Simple Way of Improving Graphite Nanoplatelets (GNP) for Their Incorporation into a Polymer Matrix. **2012**, *6* (2), 142–147. https://doi.org/10.3144/expresspolymlett.2012.15.

(29) Wang, C.; Gao, H.; Li, H.; Zhang, Y.; Huang, B.; Zhao, J.; Zhu, Y.; Yuan, W. Z.; Zhang, Y. Graphene Nanoribbons Hybridized Carbon Nanofibers: Remarkably Enhanced Graphitization and Conductivity, and Excellent Performance as Support Material for Fuel Cell Catalysts. *Nanoscale* **2014**, *6* (3), 1377–1383. https://doi.org/10.1039/c3nr04663j.

(30) Dutta, S.; Pati, S. K. Novel Properties of Graphene Nanoribbons : A Review. **2010**, 8207–8223. https://doi.org/10.1039/c0jm00261e.

(31) Salim, N. V; Jin, X.; Razal, J. M. Polyacrylonitrile / Liquid Crystalline Graphene Oxide Composite Fi Bers – Towards High Performance Carbon Fi Ber Precursors. *Compos. Sci. Technol.* **2019**, *182* (August), 107781. https://doi.org/10.1016/j.compscitech.2019.107781.

(32) Şahin, K.; Fasanella, N. A.; Chasiotis, I.; Lyons, K. M.; Newcomb, B. A.; Kamath, M. G.; Chae, H. G.; Kumar, S. High Strength Micron Size Carbon Fibers from

Polyacrylonitrile-Carbon Nanotube Precursors. *Carbon N. Y.* **2014**, *77*, 442–453. https://doi.org/10.1016/j.carbon.2014.05.049.

(33) Newcomb, B. A.; Gi, H.; Gulgunje, P. V; Gupta, K.; Liu, Y.; Tsentalovich, D. E.; Pasquali, M.; Kumar, S. Stress Transfer in Polyacrylonitrile / Carbon Nanotube Composite Fi Bers. *Polymer (Guildf).* **2014**, *55* (11), 2734–2743. https://doi.org/10.1016/j.polymer.2014.04.008.

(34) Newcomb, B. A.; Giannuzzi, L. A.; Lyons, K. M.; Gulgunje, P. V.; Gupta, K.; Liu, Y.; Kamath, M.; McDonald, K.; Moon, J.; Feng, B.; Peterson, G. P.; Chae, H. G.; Kumar, S. High Resolution Transmission Electron Microscopy Study on Polyacrylonitrile/Carbon Nanotube Based Carbon Fibers and the Effect of Structure Development on the Thermal and Electrical Conductivities. *Carbon N. Y.* **2015**, *93*, 502–514. https://doi.org/10.1016/j.carbon.2015.05.037.

(35) Chang, H.; Luo, J.; Liu, H. C.; Bakhtiary Davijani, A. A.; Wang, P. H.; Lolov, G. S.; Dwyer, R. M.; Kumar, S. Ductile Polyacrylonitrile Fibers with High Cellulose Nanocrystals Loading. *Polymer (Guildf).* **2017**, *122*, 332–339. https://doi.org/10.1016/j.polymer.2017.06.072.

(36) Chang, H.; Luo, J.; Liu, H. C.; Zhang, S.; Park, J. G.; Liang, R.; Kumar, S. Carbon Fibers from Polyacrylonitrile/Cellulose Nanocrystal Nanocomposite Fibers. *Carbon N. Y.* **2019**, *145*, 764–771. https://doi.org/10.1016/j.carbon.2019.01.045.

(37) Chang, H.; Luo, J.; Liu, H. C.; Zhang, S.; Park, J. G.; Liang, Z.; Kumar, S. Stabilization Study of Polyacrylonitrile/Cellulose Nanocrystals Composite Fibers. *ACS Appl. Polym. Mater.* **2019**, *1* (5), 1015–1021. https://doi.org/10.1021/acsapm.9b00057.

(38) Morris, E. A.; Weisenberger, M. C.; Abdallah, M. G.; Vautard, F.; Grappe, H.; Ozcan, S.; Paulauskas, F. L.; Eberle, C.; Jackson, D.; Mecham, S. J.; Naskar, A. K. High Performance Carbon Fibers from Very High Molecular Weight Polyacrylonitrile Precursors. *Carbon N. Y.* **2016**, *101*, 245–252. https://doi.org/10.1016/j.carbon.2016.01.104.

(39) Liu, H. C.; Luo, J.; Chang, H.; Bakhtiary Davijani, A. A.; Wang, P. H.; Kumar, S. Polyacrylonitrile Sheath and Polyacrylonitrile/Lignin Core Bi-Component Carbon Fiber. *Carbon N. Y.* **2019**, *149*, 165–172. https://doi.org/10.1016/j.carbon.2019.04.004.

(40) Chang, H.; Lu, M.; Luo, J.; Park, J. G.; Liang, R.; Park, C.; Kumar, S. Polyacrylonitrile/Boron Nitride Nanotubes Composite Precursor and Carbon Fibers. *Carbon N. Y.* **2019**, *147*, 419–426. https://doi.org/10.1016/j.carbon.2019.03.026.

(41) Li, S.; Chen, C.; Fu, K.; Xue, L.; Zhao, C.; Zhang, S.; Hu, Y.; Zhou, L.; Zhang, X. Comparison of Si / C , Ge / C and Sn / C Composite Nano Fi Ber Anodes Used in Advanced Lithium-Ion Batteries. **2014**, *254*, 17–26. https://doi.org/10.1016/j.ssi.2013.10.063.

(42) Mohanty, A. K.; Misra, M.; Demiro, S. Fabrication of Conductive Lignin / PAN Carbon Nano Fi Bers with Enhanced Graphene for the Modi Fi Ed Electrodes. **2019**, *147*, 262–275. https://doi.org/10.1016/j.carbon.2019.02.058.

(43) Imura, Y.; Hogan, R. M. C.; Jaffe, M. *Dry Spinning of Synthetic Polymer Fibers*; Woodhead Publishing Limited, 2014. https://doi.org/10.1533/9780857099174.2.187.

(44) Meng, F.; Lu, W.; Li, Q.; Byun, J. H.; Oh, Y.; Chou, T. W. Graphene-Based Fibers: A Review. *Adv. Mater.* **2015**, *27* (35), 5113–5131. https://doi.org/10.1002/adma.201501126.

(45) Ozipek, B.; Karakas, H. *Wet Spinning of Synthetic Polymer Fibers*; Woodhead Publishing Limited, 2014. https://doi.org/10.1533/9780857099174.2.174.

(46) Liu, Y.; Chae, H. G.; Kumar, S. Gel-Spun Carbon Nanotubes/Polyacrylonitrile Composite Fibers. Part I: Effect of Carbon Nanotubes on Stabilization. *Carbon N. Y.* **2011**, *49* (13), 4466–4476. https://doi.org/10.1016/j.carbon.2011.06.043.

(47) Chae, H. G.; Choi, Y. H.; Minus, M. L.; Kumar, S. Carbon Nanotube Reinforced Small Diameter Polyacrylonitrile Based Carbon Fiber. *Compos. Sci. Technol.* **2009**, *69* (3–4), 406–413. https://doi.org/10.1016/j.compscitech.2008.11.008.

(48) Bandopadhyay, A.; Ghosh, U. Electrohydrodynamic Phenomena. *J. Indian Inst. Sci.* **2018**, *98* (2), 201–225. https://doi.org/10.1007/s41745-018-0075-3.

(49) Ni, Q. Q.; Jin, X. D.; Xia, H.; Liu, F. Electrospinning, Processing and Characterization of Polymer-Based Nano-Composite Fibers. **2014**, 128–148. https://doi.org/10.1533/9780857099174.2.128.

(50) Yusof, N.; Ismail, A. F. Post Spinning and Pyrolysis Processes of Polyacrylonitrile (PAN)-Based Carbon Fiber and Activated Carbon Fiber: A Review. *J. Anal. Appl. Pyrolysis* **2012**, *93*, 1–13. https://doi.org/10.1016/j.jaap.2011.10.001.

(51) Rahaman, M. S. A.; Ismail, A. F.; Mustafa, A. A Review of Heat Treatment on Polyacrylonitrile Fiber. *Polym. Degrad. Stab.* **2007**, *92* (8), 1421–1432. https://doi.org/10.1016/j.polymdegradstab.2007.03.023.

(52) Tajaddod, N.; Li, H.; Minus, M. L. Low-Temperature Graphitic Formation Promoted by Confined Interphase Structures in Polyacrylonitrile/Carbon Nanotube Materials. *Polymer (Guildf).* **2018**, *137*, 346–357. https://doi.org/10.1016/j.polymer.2018.01.007.

(53) Gupta, A.; Harrison, I. R. New Aspects in the Oxidative Stabilization of Pan-Based Carbon Fibers: II. *Carbon N. Y.* **1997**, *35* (6), 809–818. https://doi.org/10.1016/S0008-6223(97)00025-0.

(54) Gutmann, P.; Moosburger-Will, J.; Kurt, S.; Xu, Y.; Horn, S. Carbonization of Polyacrylonitrile-Based Fibers under Defined Tensile Load: Influence on Shrinkage Behavior, Microstructure, and Mechanical Properties. *Polym. Degrad. Stab.* **2019**, *163*, 174–184. https://doi.org/10.1016/j.polymdegradstab.2019.03.007.

(55) Son, S. Y.; Jo, A. Y.; Jung, G. Y.; Chung, Y. S.; Lee, S. Accelerating the Stabilization of Polyacrylonitrile Fibers by UV Irradiation. *J. Ind. Eng. Chem.* **2019**, *73*, 47–51. https://doi.org/10.1016/j.jiec.2019.01.012.

(56) Bashir, Z. A Critical Review of the Stabilisation of Polyacrylonitrile. *Carbon N. Y.* **1991**, *29* (8), 1081–1090. https://doi.org/10.1016/0008-6223(91)90024-D.

(57) Ge, Y.; Fu, Z.; Deng, Y.; Zhang, M.; Zhang, H. The Effects of Chemical Reaction on the Microstructure and Mechanical Properties of Polyacrylonitrile (PAN) Precursor Fibers. *J. Mater. Sci.* **2019**, *54* (19), 12592–12604. https://doi.org/10.1007/s10853-019-03781-5.

(58) Fitzer, E.; Frohs, W.; Heine, M. Optimization of Stabilization and Carbonization Treatment of PAN Fibres and Structural Characterization of the Resulting Carbon Fibres. *Carbon N. Y.* **1986**, *24* (4), 387–395. https://doi.org/10.1016/0008-6223(86)90257-5.

(59) Saha, B.; Schatz, G. C. Carbonization in Polyacrylonitrile (PAN) Based Carbon Fibers Studied by ReaxFF Molecular Dynamics Simulations. **2012**, No. c, 2–10. https://doi.org/10.1021/jp300581b.

(60) Zhang, Y.; Tajaddod, N.; Song, K.; Minus, M. L. Low Temperature Graphitization of Interphase. *Carbon N. Y.* **2015**, *91*, 479–493. https://doi.org/10.1016/j.carbon.2015.04.088.

(61) Zhang, X.; Lu, Y.; Xiao, H. Effect of Hot Stretching Graphitization on the Structure and Mechanical Properties of Rayon-Based Carbon Fibers. **2014**, 673–684. https://doi.org/10.1007/s10853-013-7748-0.

(62) Sha, J. J.; Dai, J. X.; Li, J.; Wei, Z. Q.; Hausherr, J.; Krenkel, W. Applied Surface Science Influence of Thermal Treatment on Thermo-Mechanical Stability and Surface Composition of Carbon Fiber. **2013**, *274*, 89–94. https://doi.org/10.1016/j.apsusc.2013.02.102.

(63) Zhang, B.; Lu, C.; Liu, Y.; Zhou, P.; Yu, Z.; Yuan, S. Wet Spun Polyacrylonitrile-Based Hollow-Mesoporous Fibers with Different Draw Ratios. *Polymer (Guildf).* **2019**, *179* (May). https://doi.org/10.1016/j.polymer.2019.121618.

(64) Zhou, Z.; Liu, T.; Khan, A. U.; Liu, G. Block Copolymer–Based Porous Carbon Fibers. *Sci. Adv.* **2019**, *5* (2), 1–10. https://doi.org/10.1126/sciadv.aau6852.

(65) Salanne, M.; Rotenberg, B.; Naoi, K.; Kaneko, K.; Taberna, P.; Grey, C. P.; Dunn, B. Efficient Storage Mechanisms for Building Better Supercapacitors. **2016**, *1* (June). https://doi.org/10.1038/NENERGY.2016.70.

(66) Yang, Y.; Simeon, F.; Hatton, T. A.; Rutledge, G. C. Polyacrylonitrile-Based Electrospun Carbon Paper for Electrode Applications. **2011**. https://doi.org/10.1002/app.

(67) Ravichandran, D.; Xu, W.; Franklin, R.; Kanth, N.; Jambhulkar, S.; Shukla, S.; Song, K. Fabricating Fibers of a Porous-Polystyrene Shell and Particle-Loaded Core. *Molecules* **2019**, *24*, 4142

(68) Liu, H. C.; Luo, J.; Chang, H.; Bakhtiary, A. A.; Wang, P.; Kumar, S. Polyacrylonitrile Sheath and Polyacrylonitrile / Lignin Core Bi-Component Carbon Fi Ber. *Carbon N. Y.* **2019**, *149*, 165–172. https://doi.org/10.1016/j.carbon.2019.04.004.

(69) Chang, H.; Chien, A. T.; Liu, H. C.; Wang, P. H.; Newcomb, B. A.; Kumar, S. Gel Spinning of Polyacrylonitrile/Cellulose Nanocrystal Composite Fibers. *ACS Biomater. Sci. Eng.* **2015**, *1* (7), 610–616. https://doi.org/10.1021/acsbiomaterials.5b00161.

(70) Chae, H. G.; Minus, M. L.; Kumar, S. Oriented and Exfoliated Single Wall Carbon Nanotubes in Polyacrylonitrile. *Polymer (Guildf).* **2006**, *47* (10), 3494–3504. https://doi.org/10.1016/j.polymer.2006.03.050.

(71) Gulgunje, P. V.; Newcomb, B. A.; Gupta, K.; Chae, H. G.; Tsotsis, T. K.; Kumar, S. Low-Density and High-Modulus Carbon Fibers from Polyacrylonitrile with Honeycomb Structure. *Carbon N. Y.* **2015**, *95*, 710–714. https://doi.org/10.1016/j.carbon.2015.08.097.

(72) Wang, F.; Shao, J. Modified Weibull Distribution for Analyzing the Tensile Strength of Bamboo Fibers. **2014**, 3005–3018. https://doi.org/10.3390/polym6123005.